

Time-resolved Photolabeling of the Nicotinic Acetylcholine Receptor by [³H]Aziatomidate, an Open State Inhibitor[†]

David C. Chiara[#], Filbert H. Hong[#], Enrique Arevalo, S. Shaukat Husain, Keith W. Miller,
Stuart A. Forman, and Jonathan B. Cohen[†]

Department of Neurobiology, Harvard Medical School, Boston MA 02115 (D.C.C., F.H.H,
J.B.C.), Department of Anesthesia and Critical Care, Massachusetts General Hospital, Boston,
MA 02114 (E.A., S.S.H., K.W.M, and S.A.F.) , and Department of Biological Chemistry and
Molecular Pharmacology, Harvard Medical School, Boston, MA 02115 (K.W.M.)

Running Title: Open-state photolabeling of the nAChR

To whom correspondence should be addressed:

Jonathan B. Cohen

Dept. of Neurobiology, Harvard Medical School

220 Longwood Ave., Boston, MA 02115

Tel: (617) 432-1728; Fax: (617) 734-7557; email: jonathan_cohen@hms.harvard.edu

Text pages: 24

Tables: 2

Figures: 9

References: 40

Abstract: 249 words

Introduction: 738 words

Discussion: 1494 words

Abbreviations: nAChR, nicotinic acetylcholine receptor; azietomidate, 2-(3-methyl-3H-diaziren-3-yl)ethyl 1-(phenylethyl)-1H-imidazole-5-carboxylate; Carb, carbamylcholine; etomidate, 2-ethyl 1-(phenylethyl)-1H-imidazole-5-carboxylate; TDBzl-etomidate, 4-[3-(trifluoromethyl)-3H-diazirin-3-yl]benzyl-1-(1-phenylethyl)-1H-imidazole-5-carboxylate; TID, 3-(trifluoromethyl)-3-(m-iodophenyl)diazirine; GABA_A receptor, γ -aminobutyric acid type A receptor; V8 protease, *Staphylococcus aureus* endopeptidase Glu-C; EndoLys-C, *Lysobacter enzymogenes* endoproteinase Lys-C; SDS, sodium dodecyl sulfate; PAGE, polyacrylamide gel electrophoresis; HPLC, high pressure liquid chromatography; TPS, *Torpedo* physiological saline

ABSTRACT

Azietomidate is a photoreactive analog of the general anesthetic etomidate that acts as a nicotinic acetylcholine receptor (nAChR) non-competitive antagonist. We used rapid perfusion electrophysiological techniques to characterize the state dependence and kinetics of azietomidate inhibition of *Torpedo* nAChRs and time-resolved photolabeling to identify the nAChR binding sites occupied after exposure to [³H]azietomidate and agonist for 50 msec (open state) or at equilibrium (desensitized state). Azietomidate acted primarily as an open channel inhibitor characterized by a bimolecular association rate constant of $k_+ = 5 \times 10^5 \text{ M}^{-1}\text{sec}^{-1}$ and a dissociation rate constant of $<3 \text{ sec}^{-1}$. Azietomidate at 10 μM , when perfused with ACh, inhibited the ACh response by ~50% after 50 msec; when preincubated for 10 sec, it decreased the peak initial response by ~15%. Comparison of the kinetics of recovery of ACh responses after exposure to ACh and azietomidate or to ACh alone indicated that at subsecond times azietomidate inhibited nAChRs without enhancing the kinetics of agonist-induced desensitization. In nAChRs frozen after 50 msec exposure to agonist and [³H]azietomidate, amino acids were photolabeled in the ion channel (position M2-20 ($\alpha\text{Glu-262}$, $\beta\text{Asp-268}$, $\delta\text{Gln-276}$)), in δM1 ($\delta\text{Cys-236}$), and in $\alpha\text{MA}/\alpha\text{M4}$ ($\alpha\text{Glu-390}$, $\alpha\text{Cys-412}$) that were also photolabeled in nAChRs in the equilibrium desensitized state at ~half the efficiency. These results identify azietomidate binding sites at the extracellular end of the ion channel, in the δ subunit helix bundle, and in the nAChR cytoplasmic domain that appear similar in structure and accessibility in the open and desensitized states of the nAChR.

General anesthetics of diverse structures, including volatiles, alcohols and intravenous anesthetics, modulate the function of members of the “Cys-loop” superfamily of neurotransmitter gated ion channels either by potentiating agonist responses at inhibitory GABA_A receptors and glycine receptors or by inhibiting responses of the excitatory serotonin 5-HT₃ and nicotinic acetylcholine receptors (nAChRs) (Yamakura *et al.*, 2001; Arias *et al.*, 2002; Hemmings *et al.*, 2005). Each Cys-loop receptor is a pentamer of homologous or identical subunits that associate at a central axis that is the ion channel. Structural models can be derived from the structure of the muscle-type nAChR based upon cryoelectron microscope images of the *Torpedo* nAChR (Unwin, 2005), which provides a definition of the tertiary structure of the nAChR but lacks the resolution necessary to reliably define the positions of individual amino acids. The N-terminal half of each subunit contributes to the extracellular domain, containing the neurotransmitter binding sites that are located at subunit interfaces (α - γ and α - δ in the $\alpha_2\beta\gamma\delta$ *Torpedo* nAChR) 30 Å above the level of the membrane. Each nAChR subunit’s transmembrane domain is made up of a loose bundle of four α helices (M1-M4), with amino acids from each M2 helix contributing to the lumen of the ion channel and M4 located most peripherally and in greatest contact with lipid. The structure of nAChR transmembrane domain suggests the existence of pockets within each subunit helix bundle and at subunit interfaces that are potential binding sites for general anesthetics and other allosteric modulators.

In the absence of agonist, the nAChR exist predominately in a resting, closed channel conformation with low affinity for agonist that is in equilibrium with a non-conducting desensitized state with highest affinity for agonist. Agonist binding induces conformational transitions, within a fraction of a millisecond, to an open channel state (Maconochie and

Steinbach, 1998), and desensitization occurs in two kinetically distinct phases over times from 0.1 sec to tens of seconds (Hess *et al.*, 1983).

Mutational analyses identified positions within the M2 helices that can enhance or reduce the potency of aliphatic alcohols as open state inhibitors (Zhou *et al.*, 2000; Wenningmann *et al.*, 2001; Borghese *et al.*, 2002). Since these mutations often affect ACh gating in the absence of anesthetics, and they include substitutions both at positions oriented towards the lumen of the ion channel and towards the interior of each subunit helix bundle or the interfaces with another subunit, it is difficult to determine whether the positions contribute directly to anesthetic binding or are involved in allosteric modulation of gating.

Photoaffinity labeling provides a method to directly identify amino acids contributing to a drug binding site in a protein without any prior assumptions about the location of the site (Kotzyba-Hibert *et al.*, 1995; Vodovozova, 2007). State-dependent drug binding sites have been mapped by photolabeling *Torpedo* nAChRs in the absence of agonist (resting state), equilibrated with agonist (desensitized state), and, by the use of rapid-mixing and freeze-quench techniques (Arevalo *et al.*, 2005), in the conformations transiently stabilized by agonist (reviewed in (Mourot *et al.*, 2006)).

R(+)-Etomidate, one of the most potent general anesthetics used clinically, acts at micromolar concentrations as an anesthetic and as a potentiator of the responses to submaximal concentrations of GABA, while at concentrations above 10 μ M, it inhibits nAChRs.

Azietomidate is a photoreactive etomidate analog that is equipotent with etomidate as a general anesthetic and as a positive allosteric modulator of GABA_ARs (Husain *et al.*, 2003; Liao *et al.*, 2005). Photolabeling studies with [³H]azietomidate identified a binding site in the GABA_AR transmembrane domain at the interface between the β and α subunits (Li *et al.*, 2006). In the

Torpedo nAChR, azietomidate is equipotent with etomidate as a noncompetitive antagonist, binding with 10-fold higher affinity to the nAChR in the desensitized state than the resting state and photolabeling amino acids near the extracellular end of the ion channel domain only in the desensitized state (position M2-20: α Glu-262 and δ Gln-276) (Ziebell *et al.*, 2004). However, it is not known where (or whether) it interacts with nAChRs in the open channel state.

To provide a further definition of the diversity of binding sites and state dependence of binding of a single general anesthetic in a “Cys-loop” receptor, we use rapid perfusion electrophysiological techniques to characterize azietomidate’s state dependence and kinetics of inhibition, and we use time-resolved photolabeling to identify the nAChR binding sites occupied after exposure to [3 H]azietomidate and agonist for 50 msec (open state) compared to the desensitized state.

Materials and Methods

Materials. nAChR-rich membranes were isolated from the electric organs of *Torpedo californica* rays (Aquatic Research Consultants, San Pedro, CA) as described (Middleton and Cohen, 1991). The membranes, which contained 1-2 nmol [³H]acetylcholine (ACh) binding sites / mg protein, were stored at -80 °C in 38% sucrose / 0.02% NaN₃. Azietomidate and [³H]azietomidate (16 Ci/mmol, stored at a concentration of 14 μM in methanol at -80 °C) were synthesized as described (Husain *et al.*, 2003). Endoproteinase Lys-C (EndoLys-C) was from Roche Applied Sciences (Indianapolis, IN), TPCCK-treated trypsin was from Worthington Biochemical (Lakewood, NJ), and *Staphylococcus aureus* endopeptidase Glu-C (V8 protease) was from MP Biomedicals (Solon, OH).

Animal Use. Female *Xenopus laevis* (Xenopus One, Dexter, MI) were housed in a veterinary-supervised environment in accordance with local and federal guidelines and with the approval of the institutional research animal care committee. Oocytes were harvested via minilaparotomy from frogs anesthetized with 0.1% tricaine methanesulfonate.

Oocyte expression of *Torpedo* nAChRs. *In vitro* transcription of *T. californica* nAChR subunit specific cRNAs and the protocols for the isolation and injection of *Xenopus laevis* oocytes were carried out as described (Sullivan and Cohen, 2000). Isolated follicle-free oocytes were injected with 0.5 – 1 ng of subunit RNAs in a molar ratio of 2α/β/γ/δ, and incubated at 18 °C for 48 to 72 h prior to measurement of ACh responses. Under our experimental conditions, when responses for intact oocytes were measured by two-electrode voltage clamp, the maximal currents elicited by ACh were typically 1-2 μA. Oocytes were placed in 1 M N-methyl-D-glucamine for 5-20 min and then stripped manually of their vitelline membranes before isolation of detached patches.

Patch-Clamp Electrophysiology. Macroscopic currents were recorded from excised outside-out patches at room temperature (21-23 °C). Fire-polished micropipettes for creating patches were pulled (P-97 Flaming/Brown Micropipette Puller, Sutter Instrument Co., Novato, CA) to a resistance of 1-3 M Ω . Pipets were filled with K-100 buffer (97 mM KCl, 0.2 mM EGTA, 5 mM K-HEPES, 1 mM MgCl₂, pH = 7.5), which was also used for external solutions. Oocyte patches were voltage-clamped at -50 mV, and currents through the patch clamp amplifier (Axopatch 200A, Molecular Devices, Sunnyvale, CA) were filtered (8-pole Bessel, 1-2 kHz) and digitized at 2-5 kHz by use of a Digidata 1200 interface and pClamp 8.0 (both from Molecular Devices)

Four-channel pipet protocols. Rapid application of solutions to detached patches was achieved using a dual axis piezo-driven four barrel capillary tube (2 × 2) that allows switching between four flowing solutions, with an exchange time between adjacent solutions of <0.5 msec (Forman, 1999). Channel A of the quad tube was fed from a 100 ml syringe containing K-100 buffer; channel B contained 300 μ M ACh, fed by a 15 ml syringe. Channels C and D were fed by manifolds of six 15 ml syringes, each of which had individual valves to allow simple changes in stream contents, and these channels were used to perfuse the patch with variable concentrations of ACh, azietomidate, or combinations of ACh and azietomidate. The stability of patch responses was monitored before each experiment and after each change of agonist or antagonist concentration by a control protocol: 50 msec in buffer (channel A), followed by 800 msec exposure to 300 μ M ACh (channel B), then 150 msec in buffer, repeated 4 times with a 10-15 second delay between each iteration. To determine the ACh dose-response and the concentration dependence of azietomidate inhibition, the patch was first perfused with buffer (channel A), then switched to channel C containing either a test concentration of ACh or 300 μ M

ACh and a test concentration of azietomidate, and then returned to channel A. For each azietomidate or ACh concentration series, measurements were performed in order of increasing concentration. The amount of time spent in each step varied between experiments, and is noted in the text and figure legends. For azietomidate preincubation experiments, a patch was moved from buffer (channel A) to channel C containing azietomidate (10 μM) for a variable amount of time, and then to channel D containing 300 μM ACh and azietomidate. Recordings were averages of 4-6 sweeps, with 20-30 seconds between trials and ACh control measurements taken after each condition was tested.

Three protocols were used to determine the effects of azietomidate on the kinetics of desensitization of the nAChR response. (i) The onset and recovery from agonist-induced desensitization was determined by switching a patch from buffer to 300 μM ACh for 2 seconds, at which time the patch was returned to buffer, with the recovery of the response monitored at intervals by returning the patch briefly (50 msec) to 300 μM ACh. (ii) To determine whether azietomidate enhanced the kinetics of desensitization, the patch was moved from buffer to 300 μM ACh and 10 μM azietomidate (channel D) for 2 seconds, and then the patch was returned to buffer, with the recovery of the response monitored at intervals by return of the patch to ACh and azietomidate (channel D) for 50 msec. (iii) To test for the recovery from desensitization in the presence of azietomidate, after exposure to ACh + azietomidate (channel D) for 2 seconds, the patch was moved to 10 μM azietomidate alone (channel C), and then returned at intervals to ACh + azietomidate for 50 msec.

Data Analysis. Agonist dose response curves were fit to:

$$I = I_{\max}/[1 + (K_{\text{app}}/X)^n] \quad (1)$$

where I and I_{\max} are the current at agonist concentration x and the maximum current, respectively, K_{app} is the agonist concentration for half-maximal response, and n_H the Hill coefficient. The concentration dependence of drug inhibition of ACh-induced currents was fit to:

$$I = I_0 / [1 + (x/IC_{50})] \quad (2)$$

where I is the current in the presence of inhibitor concentration x , I_0 is the current in the absence of inhibitor, and IC_{50} is the inhibitor concentration producing 50% inhibition. SigmaPlot (SPSS) was used for the nonlinear least-squares fit of the data, and the standard errors of the parameter fits are indicated. The observed decline of the response from the peak initial response either in the presence of ACh alone (desensitization) or of ACh and azietomidate was fit to:

$$I_t = I_{\infty} + (I_{pk} - I_{\infty}) \exp^{-kt} \quad (3)$$

with I_{∞} the residual response at long times, I_{pk} , the peak initial current; and k , the rate constant.

The kinetics of recovery of the response after exposure to ACh \pm azietomidate for seconds were fit to:

$$I = I_{\text{rec}} - a_s \exp^{-bt} \quad (4)$$

with I_{rec} , the current after full recovery; a_s , the amplitude of the observed, slow recovery on the time scale of seconds; and b , the rate constant (see Figure 3A). The amplitude of the rapid phase of recovery, a_f , is equal to $I_{\text{rec}} - (a_s + I_f)$.

Photolabeling nAChR-rich membranes. For photolabeling studies, [^3H]azietomidate was isotopically diluted to 1.6 Ci/mmol with an appropriate volume of nonradioactive azietomidate at 1 mg/ml in methanol, which was removed via evaporation immediately prior to the addition of *Torpedo* physiological saline (TPS, 250 mM NaCl, 5 mM KCl, 3 mM CaCl₂, 2 mM MgCl₂, 5 mM NaPO₄, pH 7.0) with or without *Torpedo* nAChR-rich membranes resuspended at 4 mg protein/ml. The freeze-clamp apparatus and method were described

previously (Addona *et al.*, 1999; Arevalo *et al.*, 2005). Briefly, two syringes driven by a pneumatic ram are upstream of two sample loops loaded with the solutions to be mixed. When the pneumatic ram is activated, the solutions are forced through a mixer (< 1 msec) and an aging tube onto a rotating stainless steel disk pre-cooled to liquid nitrogen temperatures. Typically, one sample loop contained 0.5 ml of nAChR-membranes, sometimes premixed with [³H]azietomidate and/or agonist (carbamylcholine (Carb)), and the other contained 0.5 ml of TPS, Carb, and/or [³H]azietomidate. After mixing, the final concentrations were 2 mg membrane protein/ml, 10 μM [³H]azietomidate, and 10 mM Carb. Stainless steel tubing was used throughout. The membranes on the freezing plate, which was rotating slowly in contact with liquid nitrogen, were then irradiated (Blak-Ray UV lamp model UVL-56) for 30 min at 365 nm at a distance of ~3 cm. After irradiation, the frozen membranes were collected with pre-cooled forceps and stored at -80 °C. To obtain sufficient material for identification of labeled amino acids, material was pooled from six samples photolabeled in the frozen state in each condition, and 12 samples could be photolabeled in a day. Carb, an ACh analog resistant to hydrolysis by acetylcholinesterase, was used as the agonist for photolabeling studies because of the high concentrations of the esterase in the nAChR-rich membranes. For native *Torpedo* nAChR in sealed vesicles, Carb produces a maximal flux response close that of ACh with a concentration dependence characterized by a K_{app} of 1 mM, i.e. 20-fold higher than that of ACh (Forman *et al.*, 1987)

Gel electrophoresis and proteolytic digestions. Frozen samples (~ 1 ml and 1-2 mg protein) were thawed individually in 0.2 ml of 10% sodium dodecyl sulfate (SDS). Aliquots (~100 μl) were removed for protein assay (MicroBCA, Pierce, Rockford, IL) and analysis by analytical SDS-PAGE, and the six samples for each condition (~ 6 ml) were then pooled and

combined with 4 × sample buffer (final concentration: 8% sucrose, 2% SDS, 0.06 M Tris, 2.5% β-mercaptoethanol, 0.4% glycerol, 0.0025% bromophenol blue, pH 6.8) for isolation of nAChR subunits by SDS-PAGE on 1.5 mm thick acrylamide (8%) slab gels. Because of the large sample volumes, the loading wells were ~ 6 cm deep, and the stacking and resolving gels were ~ 3 cm and 15 cm long. After staining with Coomassie blue, the gel bands containing the β, γ, and δ subunits were excised and eluted passively for 3 days into 12 ml of elution buffer (100 mM NH₄HCO₃, 2.5 mM dithiothreitol and 0.1% SDS, pH 8.4). The bands containing the α subunit were excised and layered onto a second, 15% acrylamide gel for limited digestion “in gel” with *S. aureus* V8 protease (White and Cohen, 1988). After electrophoresis, that gel was stained with GelCode Blue (Pierce), and the proteolytic fragments of 20 kDa (αV8-20), 18 kDa (αV8-18) and 10 kDa (αV8-10) were excised and eluted. The eluates were filtered and concentrated to <400 μl by centrifugal filtration. nAChR subunits or subunit fragments were acetone precipitated in 75% acetone (12 h at -20 °C), and the pellets were resuspended in 100-200 μl of digestion buffer (15 mM Tris, 0.5 mM EDTA, 0.1% SDS, pH 8.1). Protease digests of αV8-20 and αV8-10 were fractionated directly by reversed-phase HPLC, while digests of the β and δ subunits were fractionated on 1.5 mm thick 16.5% T / 6.0% C Tricine SDS-PAGE gels (Schagger and von Jagow, 1987), which were then cut into 5 mm bands and the material eluted to identify the bands containing ³H which were then concentrated and fractionated by reversed-phase HPLC.

The αV8-20 fragment and δ subunit were digested with EndoLys-C (0.75 U in 10 μl distilled water per sample) for 2 weeks at 25 °C. For digestion with trypsin, the β subunit and the αV8-10 fragment in resuspension buffer were diluted 5-fold with 100 mM NH₄HCO₃, 0.5% Genapol C-100 (CalBiochem, San Diego, CA), pH 8.1, and trypsin (100 μg, in 20 mM CaCl₂ at

1/10 the volume of the material to be digested) was then added for digestion at 25 °C overnight (β subunit) or for 3 days (α V8-10).

Reversed-phase HPLC. Samples were fractionated using a Brownlee Aquapore BU-300 7 μ 100 \times 2.1 mm column with a NEWGUARD RP-2 7 μ guard column on an Agilent 1100 binary system with an in-line solvent degasser, a column compartment (temperature held at 40 °C), and attached UV absorbance (215 nm) and fluorescence detectors. The aqueous phase was 0.08% trifluoroacetic acid, the organic phase was 60% acetonitrile, 40% isopropanol, and 0.05% trifluoroacetic acid, the flow rate was 200 μ l/min, and the gradient used is included on HPLC trace figures as a dashed line. Fraction volumes were 500 μ l, of which 10% was assayed for 3 H.

Sequence Analysis. N-terminal sequencing was performed on a Procise[®] 492 protein sequencer (Applied Biosystems, Foster City, CA), modified such that 1/6 of the PTH-amino acid solution from each cycle was injected into the amino acid analyzer and the other 5/6 of the sample was sent to a fraction collector for 3 H quantitation. Most HPLC fractions were drop-loaded onto glass fiber filters (Applied Biosystems no. 401111) at 45 °C, with BioBrene Plus (Applied Biosystems) added after loading to avoid heat-induced peptide bond cleavage at tryptophans (Chiara *et al.*, 2003). Fractions containing α M4 or δ M1, which are not sequenced efficiently on glass fiber filters, were loaded for sequencing onto ProSorb[™] PVDF filter cartridges (Applied Biosystems no. 402052).

The amount of released PTH-derivative in each cycle, which was determined by comparison to standards from the background-corrected peak height using the model 610A Data Analysis Program, is shown in the figures along with the 3 H released in each cycle. To determine the amount of peptide in each sample, the background-subtracted number of pmol detected ($f(x)$) in cycle x was fit to the equation $f(x) = I_0 \times R^x$, and the equation was solved for I_0 (initial peptide

amount) and R (average repetitive yield). Ser, Cys, Arg, His, and Trp residues were excluded from the fit due to known problems with their quantitation. Unless otherwise noted, the efficiency of labeling of an amino acid (cpm per pmol) was calculated as $(\text{cpm}_x - \text{cpm}_{x-1}) / (5 \times I_0 R^x)$.

Molecular Modeling. The *Torpedo* nAChR structure (PDB#: 2BG9) was used to model the interactions of azietomidate with the receptor in the photolabeled regions using the Discovery Studio molecular modeling package (Accelrys, San Diego, CA). Docking studies were performed using CDocker by starting with a minimized model of azietomidate placed in existing pockets within the structure adjacent to labeled residues using a binding site sphere 15-18 Å in radius. The program then identified 100 possible solutions, and for visualization, each binding pocket was represented by the Connolly surface, defined by a 1.8 Å diameter probe, of the ensemble of the ten docking solutions with the most favorable binding energies (Figure 8).

RESULTS

nAChR inhibition by azietomidate. When ACh responses were measured by rapid perfusion of nAChRs in detached, “outside-out” patches held at -50 mV, the concentration dependence of the ACh response was characterized by a K_{app} of 40 μ M and a Hill coefficient, n_H , of 2 (Figure 1). Representative current traces are shown in Figure 1A for *Torpedo* nAChRs exposed to ACh concentrations from 10 μ M to 1 mM. ACh at 300 μ M produced a maximal response in several milliseconds, and the current response then decreased by ~20% in 100 msec. ACh at 1 mM produced a similar initial peak response, which was followed by a rapid decline of ~10%, presumably due to channel block, and then by a further decline at a rate similar to that seen at 300 μ M ACh.

To test the effects of azietomidate, nAChRs were exposed simultaneously for 800 msec to 300 μ M ACh and azietomidate at concentrations varying from 1 to 30 μ M (Figure 2). For 300 μ M ACh alone, the decline from the peak current response (agonist-induced desensitization) was well fit by a single exponential characterized by τ of 450 ± 75 msec ($n = 5$), with the current responses decreasing by ~75% after 800 msec. Exposure to increasing concentrations of azietomidate reduced the peak initial responses by less than 5%, but there was a concentration dependent increase in the rate and extent of the decline of the response from the peak. In the presence of 10 μ M azietomidate, ACh responses were inhibited by ~50% after ~60 msec and by ~98% by 800 msec. Etomidate over a similar concentration range had the same effect on ACh responses (not shown). When the concentration dependence of inhibition was quantified by measuring the net charge transfer during the 800 msec exposure period, the IC_{50} for azietomidate inhibition was 6 ± 2 μ M ($n = 4$) (Figure 2B), while for etomidate the IC_{50} was 7 ± 4 ($n = 2$).

Azietomidate at increasing concentrations enhanced the rate and extent of the decline of the ACh response. At all concentrations, that decline was well fit by a single exponential, and the rate increased linearly with azietomidate concentration (Figure 2C). While the kinetics of decline of the response in the presence of ACh alone reflects the kinetics of agonist-induced desensitization, the observed concentration-dependent inhibition by azietomidate could reflect either enhanced kinetics of desensitization or the kinetics of binding of azietomidate. Assuming the latter case, the observed inhibition would be consistent with an apparent bimolecular association rate constant for azietomidate of $(5.0 \pm 0.2) \times 10^5 \text{ M}^{-1}\text{sec}^{-1}$ (data from 3 patches). Additional experiments, described below, establish that the nAChRs inhibited by azietomidate are not in the desensitized state that is stabilized by agonist.

Preincubation with azietomidate had only subtle effects on the inhibition of the ACh response (Figure 2D). Prior exposure to 10 μM azietomidate for either 5 or 10 sec resulted in a decrease of the peak initial response by ~15% and a doubling in the rate of decline of the ACh response compared to simultaneous addition.

Recovery from inhibition. To determine whether azietomidate stabilized the same nAChR desensitized state as ACh, we measured the kinetics of recovery of ACh responses after exposure to 300 μM ACh alone for 2 sec or to ACh and 10 μM azietomidate (Figure 3). The general features of the ACh response expected for such a protocol are schematized in Figure 3A, and experimental data are shown for patches exposed only to buffer during the recovery period (Figure 3B) or exposed to 10 μM azietomidate throughout the recovery period (Figure 3C), with the parameters characterizing the recovery kinetics in Table 1.

After exposure to either ACh or ACh and azietomidate, recovery occurred in two phases: a rapid phase (amplitude, a_r), complete within 100 msec, and a slow phase (amplitude, a_s),

characterized by $\tau_s \sim 0.7$ sec). For the ACh controls, the response decreased by 70% during the 2 sec application of ACh, while in the presence of ACh and azietomidate, the response decreased to baseline. For the ACh controls, 80-85% of the recovery occurred during the slow phase. After exposure to ACh and azietomidate, the observed recovery was similar whether or not azietomidate was present during the recovery phase. In both conditions, after 100 msec recovery, the ACh response was close to that seen after desensitization by ACh alone. Thus, the rapid phase of recovery was larger after exposure to ACh and azietomidate than to ACh alone, while the slow phase occurred with an amplitude and kinetics similar to that seen for ACh alone. These results establish that when azietomidate inhibits the nAChR in the presence of ACh, it does not do so by stabilizing the ACh-induced desensitized state.

Comparison of nAChR inhibition by azietomidate and QX-222. To further characterize the state of the nAChR inhibited by azietomidate, two additional rapid perfusion protocols were used to compare nAChR by azietomidate with inhibition by QX-222, which acts as an open channel blocker characterized by rapid association and dissociation ($k_+ = 4 \times 10^7 \text{ M}^{-1}\text{s}^{-1}$, $k_- = 1 \times 10^3 \text{ s}^{-1}$ (Dilger and Vidal, 1994)). In one protocol, nAChRs were exposed to ACh and QX-222 or azietomidate and then returned to buffer. After exposure to ACh and QX-222, the current was ~30% of control (ACh alone) after 30 msec, and a transient increase in current (“rebound” current) was seen after the patch was moved to buffer, which results from ion flow through open channels as QX-222 dissociates (Figure 4A). For nAChRs exposed to 300 μM ACh and 10 μM azietomidate, the current was at ~50% of control (ACh alone) after 100 ms, and when the patch was then switched to buffer, the current decreased within milliseconds to baseline without evidence of any “rebound” current (Figure 4C). Thus, azietomidate did not act as an open channel blocker characterized by rapid dissociation.

In a second protocol, responses were measured when the patch was shifted from ACh and QX-222 or azietomidate to ACh alone. After exposure to ACh and QX-222 for 30 msec, when the patch was returned to ACh, the current rapidly increased to the level seen for ACh alone (Figure 4B), which indicates that QX-222 dissociates rapidly from nAChRs that had been inhibited without any increase in the fraction in the desensitized state. When the patch was moved to a stream of ACh after 30 msec exposure to ACh and azietomidate, the current neither increased to control levels as seen for QX-222 nor declined as in the continued presence of azietomidate. Rather, the current response declined at a rate similar to the control ACh response (Figure 4D). This response suggests that the nAChRs that had bound azietomidate within 30 msec remained occupied and inhibited during the subsequent 200 msec exposure to ACh, while ACh binding to the nAChRs that had not bound azietomidate resulted in channel gating and then desensitization.

[³H]Azietomidate photolabeling of nAChRs frozen after 50 msec exposure to agonist.

For nAChRs exposed to an agonist concentration producing a maximal response, the electrophysiological analyses established that there was little desensitization within 50 msec and that simultaneous exposure to 10 μ M azietomidate inhibited the response by ~50%, with no evidence that the inhibition was associated with stabilization of nAChRs in the slowly reversible desensitized state stabilized by agonist. Therefore, to characterize [³H]azietomidate photolabeling when a maximal fraction of nAChRs are in the open state, nAChRs were frozen for photolabeling 50 msec after exposure to [³H]azietomidate at a final concentration of 10 μ M and with the agonist carbamylcholine (Carb) at a concentration (10 mM) which produces a maximal response for native *Torpedo* nAChRs in sealed vesicles (Forman *et al.*, 1987). This photolabeling condition will be referred to as “**Open**”, although these nAChRs will be

distributed in the multiple conformational states transiently stabilized by agonist (open, “pre-open” (Lape *et al.*, 2008), and fast-desensitized). In parallel, nAChRs pre-equilibrated with 10 mM Carb were photolabeled when frozen after 50 msec exposure to 10 μ M [3 H]azietomidate and 10 mM Carb (**Des**, agonist desensitized state). Table 2 summarizes for comparison purposes the efficiencies (cpm/mol) of [3 H]azietomidate photolabeling of nAChR amino acids in each of the photolabeling conditions.

Photolabeled amino acids in the α subunit transmembrane domain were identified by isolating labeled fragments from proteolytic digests of two large subunit fragments that are produced by digestion “in gel” with V8 protease (White and Cohen, 1988): a 10 kDa fragment (α V8-10, beginning at α Asn-339 and containing α M4) and a 20 kDa fragment (α V8-20, beginning at α Ser-162/173 and containing M1-M3). When the trypsin digest of α V8-10 was fractionated by reversed-phase HPLC (Figure 5A), ~80% of 3 H was recovered in or near the flow-through fractions, and ~20% was recovered in a broad hydrophobic peak (70-95% organic) that is known to contain the fragments spanning α M4. Sequence analysis of the pool of the hydrophobic peak (Figure 5B) revealed the presence of a primary sequence beginning at α Ser-388, extending through α Lys-400 and α M4, and a secondary sequence beginning at α Tyr-401. The major peak of 3 H release was in cycle 3, with a smaller peak of release in cycle 12. The 3 H release in cycle 3 resulted from labeling of α Glu-390 in the primary sequence (**Open**, 1.2 cpm/pmol; **Des**, 0.6 cpm/pmol), since labeling of α Ala-403 in the secondary sequence would have also resulted in a peak of 3 H release in cycle 16 from the primary sequence, which was not seen. The 3 H release in cycle 12 probably resulted from labeling of α Cys-412 in the secondary sequence (**Open**, 0.9 cpm/pmol; **Des**, 0.5 cpm/pmol), since there were also low peaks of 3 H release in cycle 25. Since [3 H]azietomidate photolabels α Glu-390, at least some of the 3 H in the

HPLC flow-through fractions of Figure 5A must result from the presence of labeled α Glu-390 in the hydrophilic peptides also generated when α V8-10 is cleaved at α Glu-400 to produce the fragment beginning at α Tyr-401. However, additional studies are required to determine whether [3 H]azietomidate photolabels other amino acids between α Asn-339 and α Glu-387 that would also be contained within the hydrophilic fragments produced by trypsin cleavage of α V8-10.

To identify the amino acids photolabeled in α V8-20, digestion with EndoLys-C was used, which generates fragments beginning at α His-186, containing α M1, and at α Met-242, containing M2 and M3, which can be resolved by reversed-phase HPLC (Ziebell *et al.*, 2004). When the EndoLys-C digests of α V8-20 were fractionated by reversed-phase HPLC (Figure 5C), ~20% of 3 H was recovered in a hydrophobic peak centered at 90% organic, which by sequence analysis contained the fragment beginning at α Met-242 as the primary sequence and a single peak of 3 H release in cycle 20 corresponding to labeling of α Glu-262 (**Open**, 25 cpm/pmol; **Des**, 13 cpm/pmol) (Figure 5D).

To identify the amino acids photolabeled in the δ subunit transmembrane domain, the photolabeled δ subunits were digested with EndoLys-C, which generates fragments of 10-14 kDa, one beginning at δ Phe-206 and containing δ M1 and another beginning at δ Met-257 at the N-terminus of δ M2 and extending through δ M3, that can be separated by reversed-phase HPLC after fractionation of the digests by Tricine-SDS PAGE (Arevalo *et al.*, 2005). When the materials from these gel bands (Figure 6A) were pooled and fractionated by reversed-phase HPLC (Figure 6B), ~60% of 3 H was recovered in a peak at ~75% organic that contained the fragment beginning at δ Met-257 as the primary sequence, and ~10% of 3 H was recovered in fractions eluting at ~60% organic that contained the fragment beginning at δ Phe-206. For the

fragment beginning at δ Met-257, there was a major peak of ^3H release in cycle 20 (Figure 6C), consistent with photolabeling of δ M2-20 (δ Gln-276; **Open**, 1 cpm/pmol; **Des**, 0.3 cpm/pmol). For the fragment beginning at δ Phe-206 (Figure 6D), a single peak of ^3H release in cycle 31 indicated labeling within δ M1 of δ Cys-236 (**Open**, 0.7 cpm/pmol; **Des**, 0.2 cpm/pmol).

Frozen-state photolabeling of nAChRs equilibrated with [^3H]azietomidate. To compare with our previous results obtained with nAChRs in the desensitized state photolabeled in solution (Ziebell *et al.*, 2004), we photolabeled nAChRs in the frozen state that had been equilibrated in solution with [^3H]azietomidate (18 μM) in the presence of a high concentration of 10 mM Carb, and then mixed with 10 mM Carb and frozen after 50 msec exposure. Membranes equilibrated with [^3H]azietomidate in the absence of agonist and then frozen after 50 msec exposure to Carb were also photolabeled in parallel.

To identify the amino acids photolabeled within α M2, the fragment beginning at α Met-242 at the N-terminus of α M2 was isolated by reversed-phase HPLC from an EndoLys-C digest of α V8-20. Sequence analysis of that fragment (Figure 7A) revealed a single major peak of ^3H release in cycle 20, corresponding to the labeling of α Glu-262. For nAChRs pre-equilibrated with [^3H]azietomidate and Carb (desensitized state), α Glu-262 was labeled at 40 cpm/pmol, while for the samples pre-equilibrated with [^3H]azietomidate alone and then exposed to Carb for 50 msec, α Glu-262 was labeled at 70 cpm/pmol.

To identify the amino acids photolabeled in δ M2, the beginning at δ Met-257 at the N-terminus of δ M2 was purified by reversed-phase HPLC after fractionation of the δ subunit digest by Tricine-SDS PAGE. Sequence analysis of the fragment beginning at δ Met-257 (Figure 7B) revealed a single peak of ^3H release in cycle 20, consistent with labeling of δ Gln-276 at 1 cpm/pmol for the sample photolabeled in the desensitized state, and at 2 cpm/pmol for the

sample pre-equilibrated with [^3H]azietomidate alone. While for nAChRs photolabeled in solution $\delta\text{M}2\text{-}2$ and $\delta\text{M}2\text{-}6$ were labeled at 10% and 5% the level of $\delta\text{M}2\text{-}20$, for nAChRs photolabeled in the frozen state, the labeling of those positions, if it occurred, was at less than 5% the labeling of $\delta\text{M}2\text{-}20$.

We also characterized [^3H]azietomidate photolabeling within $\beta\text{M}2$, which had not been characterized previously. Digestion of the β subunit with trypsin generates an ~10 kDa fragment beginning at $\beta\text{Met}\text{-}249$, the N-terminus of $\beta\text{M}2$, that can be isolated by Tricine-SDS-PAGE and HPLC purification (White and Cohen, 1992). For that fragment, which was sequenced only from nAChRs photolabeled after equilibration with [^3H]azietomidate in the absence of Carb, there was also only a single peak of ^3H release in cycle 20, consistent with labeling of $\beta\text{Asp}\text{-}268$ at 4 cpm/pmol, i.e. at a similar efficiency as $\delta\text{Gln}\text{-}276$ and at ~5% the efficiency of $\alpha\text{Glu}\text{-}262$.

DISCUSSION

We use rapid-perfusion electrophysiological techniques to establish that azietomidate acts primarily as a nAChR open state inhibitor without enhancing the kinetics of desensitization. Full inhibition by 10 μ M azietomidate develops within a second in the presence of ACh without any increase in the fraction of nAChRs in the desensitized state beyond that seen for ACh alone, and after removal of ACh, azietomidate did not stabilize nAChRs in the desensitized state. Because substantial inhibition develops after exposure to agonist and 10 μ M azietomidate for 50 msec, these conditions were chosen for time-resolved photolabeling. Further studies, requiring a combination of single channel and rapid perfusion analyses, will be required to determine whether nAChR inhibition results from physical occlusion of the ion channel or from stabilization of the nAChR in a novel, non-conducting state.

The observed concentration-dependent increase in the rate of inhibition by azietomidate indicates that its apparent rate constant for open state inhibition ($k_+ = 5 \times 10^5 \text{M}^{-1} \text{s}^{-1}$) is ~100-fold lower than that of the positively charged QX-222 (Dilger and Vidal, 1994) and ~10-fold lower than that of octanol and pentobarbital (Forman *et al.*, 1995; Dilger *et al.*, 1997). One factor that may account for azietomidate's low apparent rate constant is that it has a substantially higher lipid solubility (octanol/water partition coefficient, $P = 3600$) than octanol ($P = 1400$) or pentobarbital ($P = 130$). If the aqueous concentration determines the rate of inhibition, our calculation underestimates the value of k_+ . Slow onset and recovery from inhibition are also reported for propofol ($P = 4300$, Dilger *et al.*, 1994).

nAChR photolabeling by [³H]azietomidate. In the nAChR structure (Fig. 8), the photolabeled amino acids are distributed in 4 different structural domains: (i) at the extracellular end of the ion channel (α M2-20, β M2-20, and δ M2-20); (ii) within the δ subunit helix bundle

(δ Cys-236 in δ M1); (iii) in the cytoplasmic basket formed by the MA helices that precede the M4 helices in the primary structure (α Glu-390); and (iv) at the lipid interface (α Cys-412 in α M4). Also included in Figure 8 are Connolly surface representations (see Materials and Methods) of predicted azietomidate binding pockets within the ion channel near M2-20 (white), in the δ subunit helix bundle (blue), and in the nAChR cytoplasmic basket domain (yellow). Table 2 compares the efficiencies of [3 H]azietomidate incorporation in these structural domains. While α Glu-262 is the residue photolabeled most efficiently, and it is plausible that binding to the extracellular end of the ion channel accounts for the functional inhibition of the nAChR, occupancy at the other sites could also contribute to inhibition. Additional photolabeling over a range of azietomidate concentrations would be required to determine the relative occupancy of each site.

The time-resolved photolabeling data in Table 2 show that the accessibility at the extracellular end of the ion channel and at the other sites are similar in the state(s) transiently stabilized by agonist and in the equilibrium desensitized state, because the same amino acids in each domain are photolabeled in both states at efficiencies that differ by less than three-fold. However, [3 H]azietomidate cannot access the ion channel in the resting state (Ziebell *et al.*, 2004). The other sites were not characterized in that study.

Photolabeling in the nAChR ion channel. Photolabeling of the nAChR with [3 H]azietomidate and other aliphatic diazirines has established that the activated intermediates react most efficiently with nucleophilic side chains (Glu, Asp, Tyr) (Pratt *et al.*, 2000; Ziebell *et al.*, 2004; Hamouda *et al.*, 2006). Thus, the pattern of labeling of the glutamates and aspartates at the outer end of the channel (Table 2) likely delineates the binding pocket and orientation of azietomidate. That all of the M2-20, but none of the M2-24 (β Glu-272, δ Glu-280) residues

examined were photolabeled suggests that the pocket extends down the channel which is lined by hydrophobic residues for ~15Å (Figures 8B-C). The homologous region in GABA_ARs is lined with polar residues, providing a rationale for the much higher concentrations of azietomidate required to inhibit GABA_ARs. Orientation may also explain why αGlu-262 is labeled >10-fold more efficiently than βM2-20 (βAsp-268), because there is no obvious structural or photochemical explanation. However, we cannot rule out the possibility that the unlabeled acidic side chains at position M2-24, which are oriented towards the channel in the resting state structure, have moved in the photolabeled conformations.

Aziotanol also photolabels αM2-20 (αGlu-262) in the desensitized state (Pratt *et al.*, 2000), and mutational analyses associate irreversible nAChR inhibition with reaction at αGlu-262 (Forman *et al.*, 2007).

All of the above results are consistent with the preferred binding site for azietomidate being at the extracellular end of the ion channel. An alternative interpretation, based upon photolabeling studies of the nAChR in solution (Ziebell *et al.*, 2004), was that the reactive amino acids at the extracellular end of the channel reacted with photoactivated azietomidate as it diffused into or out of an equilibrium binding site at the cytoplasmic end of the ion channel. This possibility was based upon the photolabeling of amino acids at the cytoplasmic end of the ion channel (Ser/Thr at positions M2-2 and M2-6 of the α and δ subunits) at ~1% the efficiency of αGlu-262 (Fig. 6C). In the frozen state photolabeling, however, the equilibrium binding is trapped and there would be no ongoing transient diffusion past M2-20.

Photolabeling in the δ subunit helix bundle. The photolabeling in the presence of agonist of δM1 Cys-236, a residue that projects within the helix bundle, suggests that [³H]azietomidate binds therein. In previous studies at 20 °C, the fragment containing δM1 was photolabeled by

[³H]azietomidate in nAChRs in the desensitized, but not in the resting state (Ziebell *et al.*, 2004). Within the nAChR structure (Figures 8C and D), which is believed to be the closed state, the pocket at the extracellular end of the δ subunit helix bundle, capped by the M2-M3 loop, is large enough to accommodate azietomidate, but it ends ~ 10 Å above the level of the labeled δ Cys-236, suggesting that activation causes the structure to change in this region.

Two other nAChR inhibitors photolabel within the δ subunit helix bundle in an agonist-dependent manner: [¹²⁵I]TID photolabels δ Cys-236, δ Phe-232, δ Thr-274 (M2-18), δ Leu-278 (M2-22), and δ Ile-288 (M2-M3 loop) at least 10-times more efficiently after transient exposure to agonist than in the equilibrium desensitized state (Arevalo *et al.*, 2005; Hamouda *et al.*, 2008), and [³H]benzophenone photolabels δ Phe-232, δ Pro-286, and δ Ile-288 at 20°C only in the presence of agonist (Garcia *et al.*, 2007). However, the dramatic difference in [¹²⁵I]TID photolabeling between the transient and equilibrium agonist-stabilized states is in contrast to the <3-fold difference seen for [³H]azietomidate photolabeling within the helix bundle. While TID (vol. 150 Å³) and benzophenone (vol. 125 Å³) are both smaller than azietomidate (vol. 240 Å³), TDBzl-etomidate (vol. 284 Å³), a larger aryl diazine, did not photolabel the δ subunit helix bundle in either resting or desensitized state (Nirthanan *et al.*, 2008).

Photolabeling in the nAChR cytoplasmic domain. Azietomidate photolabeling of α Glu-390, within the basket formed by the MA helices that surround the cytoplasmic access to the ion channel (Figures 8A), provides the first evidence that this region can act as a drug binding site. α Glu-390 is ~ 25 Å below the entry to the ion channel and oriented towards the interior of the basket near the base of the portals between each of the MA helices, where the basket dimensions are appropriate for an azietomidate binding site (Figure 9). This is unlikely to be a random photolabeling event because azietomidate did not photolabel other negatively charged side

chains in this region: α Asp-389, α Glu-391, α Glu-397, or α Glu-398. However, its affinity is likely to be lower than that of the channel because of the relative degree of photoincorporation in the two regions (Table 2). Further studies will be required to explore the site's functional significance, but we note that it is close to residues that control channel conductance in the $\alpha 4\beta 2$ neuronal nAChR and the 5-HT_{3A} receptor (Hales *et al.*, 2006).

General anesthetic actions on Cys-loop receptors. While azietomidate likely inhibits the nAChR via the ion channel site, our results provide direct evidence of the diversity of binding sites even for a single general anesthetic in a Cys-loop receptor. Anesthetic binding sites in GABA_A and glycine receptors have been predicted to exist in the transmembrane domain within the pockets within the subunit helix bundles, where the volume of substituted side chains determine the “cut-off” for the size of active anesthetics (Wick *et al.*, 1998; Krasowski *et al.*, 2001). [¹⁴C]halothane (vol. 86 Å³) binds within the nAChR δ subunit helix bundle in the absence or presence of agonist, while [³H]azietomidate binds only in the presence of agonist, and the slightly larger [³H]TDBzl-etomidate does not bind there but instead binds in the pocket at the interface between the α and γ subunits (Nirathanan *et al.*, 2008). Our identification of an unexpected azietomidate binding site within the MA helix basket suggests that it will be important to determine whether this site is relevant for the action of anesthetics in other Cys-loop receptors.

REFERENCES

- Addona GH, Kloczewiak MA and Miller KW (1999) Time-resolved photolabeling of membrane proteins: application to the nicotinic acetylcholine receptor. *Anal Biochem* **267**: 135-140.
- Arevalo E, Chiara DC, Forman SA, Cohen JB and Miller KW (2005) Gating-enhanced accessibility of hydrophobic sites within the transmembrane region of the nicotinic acetylcholine receptor's delta-subunit - a time-resolved photolabeling study. *J Biol Chem* **280**: 13631-13640.
- Arias HR, Kem WR, Trudell JR and Blanton MP (2002) Unique general anesthetic binding sites within distinct conformational states of the nicotinic acetylcholine receptor. *Int Rev Neurobiol* **54**: 1-50.
- Borghese CM, Ali DN, Bleck V and Harris RA (2002) Acetylcholine and alcohol sensitivity of neuronal nicotinic acetylcholine receptors: mutations in transmembrane domains. *Alcohol Clin Exp Res* **26**: 1764-1772.
- Chiara DC, Trinidad JC, Wang D, Ziebell MR, Sullivan D and Cohen JB (2003) Identification of amino acids in the nicotinic acetylcholine receptor agonist binding site and ion channel photolabeled by 4-[(3-trifluoromethyl)-3H-diazirin-3-yl]benzoylcholine, a novel photoaffinity antagonist. *Biochemistry* **42**: 271-283.
- Dilger JP and Vidal AM (1994) Cooperative interactions between general anesthetics and QX-222 within the pore of the acetylcholine receptor ion channel. *Mol Pharmacol* **46**: 169-175.
- Dilger JP, Vidal AM, Mody HI, Liu Y (1994) Evidence for direct actions of general anesthetics on an ion channel protein. *Anesthesiology* **81**: 431-442.
- Dilger JP, Boguslavsky R, Barann M, Katz T and Vidal AM (1997) Mechanisms of barbiturate inhibition of acetylcholine receptor channels. *J Gen Physiol* **109**: 401-414.

- Forman SA (1999) A hydrophobic photolabel inhibits nicotinic acetylcholine receptors via open-channel block following a slow step. *Biochemistry* **38**: 14559-14564.
- Forman SA, Firestone LL and Miller KW (1987) Is agonist self-inhibition at the nicotinic acetylcholine receptor a nonspecific action? *Biochemistry* **26**: 2807-2814.
- Forman SA, Miller KW and Yellen G (1995) A discrete site for general anesthetics on a postsynaptic receptor. *Mol Pharmacol* **48**: 574-581.
- Forman, SA, Zhou, QL, and Stewart, DS (2007) Photoactivated 3-azidoctanol irreversibly desensitizes muscle nicotinic ACh receptors *via* interactions at α E262. *Biochemistry* **46**: 11911-11918.
- Garcia, G III, Chiara, DC, Nirthanan, S, Hamouda, AK, Stewart, DS, and Cohen, JB (2007) [³H]Benzophenone photolabeling identifies state-dependent changes in nicotinic acetylcholine receptor structure. *Biochemistry* **46**: 10296-10307.
- Hales TG, Dunlop JI, Deeb TZ, Carland JE, Kelley SP, Lambert JJ and Peters JA (2006) Common determinants of single channel conductance within the large cytoplasmic loop of 5-hydroxytryptamine type 3 and alpha(4)beta(2) nicotinic acetylcholine receptors. *J Biol Chem* **281**: 8062-8071.
- Hamouda, AK, Chiara, DC, Blanton, MP, and Cohen, JB (2008) Probing the structure of the affinity-purified and lipid-reconstituted *Torpedo* nicotinic acetylcholine receptor. *Biochemistry* **47**: 12787-12794.
- Hamouda AK, Chiara DC, Sauls D, Cohen JB and Blanton MP (2006) Cholesterol interacts with transmembrane alpha-helices M1, M3, and M4 of the *Torpedo* nicotinic acetylcholine receptor: photolabeling studies using [³H]azicholesterol. *Biochemistry* **45**: 976-986.

- Hemmings HC, Akabas MH, Goldstein PA, Trudell JR, Orser BA and Harrison NL (2005)
Emerging molecular mechanisms of general anesthetic action. *Trends Pharmacol Sci* **26**:
503-510.
- Hess, GP, Cash, DJ, and Aoshima, H (1983) Acetylcholine receptor-controlled ion translocation:
Chemical kinetic investigations of the mechanism. *Ann Rev Biophys Bioeng* **12**: 443-473.
- Husain SS, Ziebell MR, Ruesch D, Hong F, Arevalo E, Kosterlitz JA, Olsen RW, Forman SA,
Cohen JB and Miller KW (2003) 2-(3-Methyl-3*H*-diaziren-3-yl)ethyl 1-(1-phenylethyl)-1*H*-
imidazole-5- carboxylate: a derivative of the stereoselective general anesthetic etomidate for
photolabeling ligand-gated ion channels. *J Med Chem* **46**: 1257-1265.
- Kotzyba-Hibert F, Kapfer I and Goeldner M (1995) Recent trends in photoaffinity labeling.
Angew Chem Int Ed **34**: 1296-1312.
- Krasowski MD, Nishkawa K, Nikolaeva N, Lin A, and Harrison NL (2001) Methionine 286 in
transmembrane domain 3 of the GABA_A receptor β subunit controls a binding cavity for
propofol and other alkylphenol general anesthetics. *Neuropharmacol* **41**: 952-964.
- Lape, R., Colquhoun, D., and Sivilotti, LG (2008) On the nature of partial agonism in the
nicotinic receptor superfamily. *Nature* **454**: 722-727.
- Li, G-D, Chiara, DC, Sawyer, GW, Husain, SS, Olsen, RW, and Cohen, JB (2006) Identification
of a GABA_A receptor anesthetic binding site at subunit interfaces by photolabeling with an
etomidate analog. *J Neurosci* **26**: 11599-11605.
- Liao, M, Sonner, JM, Husain, SS, Miller, KW, Jurd, R, Rudolph, U, and Eger, EIR (2005) (+)
Etomidate and the photoactivable R (+) azietomidate have comparable anesthetic activity in
wild-type mice and comparably decreased activity in mice with a N265M point mutation in
the gamma-aminobutyric acid receptor β 3 subunit. *Anesthesia and Analgesia* **101** 131-135.

- Maconochie DJ and Steinbach JH (1998) The channel opening rate of adult- and fetal-type mouse muscle nicotinic receptors activated by acetylcholine. *J Physiol-London* **506**: 53-72.
- Middleton RE and Cohen JB (1991) Mapping of the acetylcholine binding site of the nicotinic acetylcholine receptor: [³H]-nicotine as an agonist photoaffinity label. *Biochemistry* **30**: 6987-6997.
- Mourot A, Grutter T, Goeldner M and Kotzyba-Hibert F (2006) Dynamic structural investigations on the *Torpedo* nicotinic acetylcholine receptor by time-resolved Photoaffinity labeling. *Chembiochem* **7**: 570-583.
- Nirathanan, S., Garcia, G III, Chiara, DC, Husain, SS, and Cohen, JB (2008) Identification of binding sites in the nicotinic acetylcholine receptor for TDBzl-etomidate, a photoreactive positive allosteric effector. *J Biol Chem* **283**: 22051-22062.
- Pratt MB, Husain SS, Miller KW and Cohen JB (2000) Identification of sites of incorporation in the nicotinic acetylcholine receptor of a photoactivatable general anesthetic. *J Biol Chem* **275**: 29441-29451.
- Schagger H and von Jagow G (1987) Tricine-sodium dodecyl sulfate-polyacrylamide gel electrophoresis for the separation of proteins in the range From 1 to 100 kDa. *Anal Biochem* **166**: 368-379.
- Sullivan DA and Cohen JB (2000) Mapping the agonist binding site of the nicotinic acetylcholine receptor: orientation requirements for activation by covalent agonist. *J Biol Chem* **275**: 12651-12660.
- Unwin N (2005) Refined structure of the nicotinic acetylcholine receptor at 4 Å resolution. *J Mol Biol* **346**: 967-989.

- Vodovozova EL (2007) Photoaffinity labeling and its application in structural biology. *Biochemistry-Moscow* **72**: 1-20.
- Wenningmann I, Barann M, Vidal AM and Dilger JP (2001) The effects of isoflurane on acetylcholine receptor channels: 3. effects of conservative polar-to-nonpolar mutations within the channel pore. *Mol Pharmacol* **60**: 584-594.
- White BH and Cohen JB (1988) Photolabeling of membrane-bound *Torpedo* nicotinic acetylcholine receptor with the hydrophobic probe 3-trifluoromethyl-3-(m-[¹²⁵I]iodophenyl)diazirine. *Biochemistry* **27**: 8741-8751.
- White BH and Cohen JB (1992) Agonist-induced changes in the structure of the acetylcholine receptor M2 regions revealed by photoincorporation of an uncharged nicotinic non-competitive antagonist. *J Biol Chem* **267**: 15770-15783.
- Wick MJ, Mihic SJ, Ueno S, Mascia MP, Trudell JR, Brozowski SJ, Ye Q, Harrison NL and Harris RA (1998) Mutations of gamma-aminobutyric acid and glycine receptors change alcohol cutoff: evidence for an alcohol receptor? *Proc Natl Acad Sci USA* **95**: 6504-6509.
- Yamakura T, Bertaccini E, Trudell JR and Harris RA (2001) Anesthetics and ion channels: molecular models and sites of action. *Ann Rev Pharmacol Toxicol* **41**: 23-51.
- Zhou QL, Zhou Q and Forman SA (2000) The n-alcohol site in the nicotinic receptor pore is a hydrophobic patch. *Biochemistry* **39**: 14920-14926.
- Ziebell MR, Nirathanan S, Husain SS, Miller KW and Cohen JB (2004) Identification of binding sites in the nicotinic acetylcholine receptor for [³H]azietomidate, a photoactivatable general anesthetic. *J Biol Chem* **279**: 17640-17649.

FOOTNOTES:

†This research was supported in part by the National Institutes of Health [Grant GM-58448] and by an award to Harvard Medical School from the Howard Hughes Biomedical Research Support Program for Medical Schools.

#These two authors contributed equally to this work.

Address correspondence to:

Jonathan B. Cohen

Department of Neurobiology, Harvard Medical School, 220 Longwood Ave, Boston, MA 02115.

E-mail: jonathan_cohen@hms.harvard.edu

FIGURE LEGENDS

Figure 1. Responses to ACh measured by rapid perfusion of *Torpedo* nAChRs in detached patches. **A**, representative macroscopic current responses when an “outside-out” patch at a holding potential of -50 mV was exposed to varying concentrations of ACh for 100 msec. Each trace is the average of 4 sweeps, with 20 seconds between each sweep. **B**, the concentration dependence of the peak ACh responses, with data from 2 patches normalized to the response to 300 μ M ACh and the error bars indicating the range. The response was fit by $K_{app} = 43 \pm 4 \mu$ M and $n_H = 1.9 \pm 0.2$.

Figure 2. Azietomidate inhibition of *Torpedo* nAChRs. Azietomidate inhibition of ACh responses of *Torpedo* nAChRs expressed in *Xenopus* oocytes was measured by rapid perfusion of outside-out patches detached from oocytes. **Panel A**, representative macroscopic current traces from a single patch exposed for 800 ms to 300 μ M ACh coapplied with increasing concentrations of azietomidate. For each concentration, the current traces are the average of 4 repetitions, with 10 sec between each sweep. Each trace was normalized to the peak current response for 300 μ M ACh applied before each exposure to azietomidate. After exposure to 30 μ M azietomidate and 10 sec recovery, the peak ACh current was >90% of the previous control, and τ_{des} was decreased by <20% compared to the value before exposure to any azietomidate. **Panel B**, the concentration dependence of azietomidate inhibition. Responses were measured by the net charge transfer during 800 msec exposure to ACh and azietomidate, normalized for each patch to the value for ACh alone. Data are the mean \pm SEM from four patches, and the calculated IC_{50} was $5.6 \pm 0.2 \mu$ M. **Panel C**, dependence of the kinetics of inhibition on azietomidate concentration. For each concentration of azietomidate, the observed decline of the

response from the peak was fit to a single exponential: $I_t = I_\infty + (I_{pk} - I_\infty) \exp^{-kt}$, with I_∞ the residual response at long times, I_{pk} , the peak initial current; and k , the rate constant. Inhibition rates (mean \pm SEM, 3 patches) are plotted against azietomidate concentration. Linear least squares regression gives a slope of $(5.0 \pm 0.2) \times 10^5 \text{ M}^{-1} \text{ sec}^{-1}$. **Panel D**, effect of azietomidate preincubation on the inhibition of *Torpedo* nAChRs in excised patches. The responses of nAChRs exposed to 300 μM ACh and 10 μM azietomidate are shown for a single patch. Prior to each ACh application, the patch was perfused with 10 μM azietomidate for 0, 5, or 10 seconds. The calculated net charge transfer during the 1-second response was 2.0 nC for the control in the absence of azietomidate, and 1.1, 0.54, and 0.48 nC following 0, 5, and 10 seconds of preincubation.

Figure 3. Recovery of ACh responses after inhibition by azietomidate. Panel A, a schematic defining the parameters characterizing the kinetics of recovery of ACh responses following exposure to ACh in the absence or presence of azietomidate. After exposure to a stream of ACh \pm azietomidate, the patch was switched to a stream containing buffer, with ACh sensitivity monitored by moving the patch for 50 ms into 300 μM ACh + azietomidate after 0.1, 0.3, 1.0, and 3.0 seconds of recovery. I_0 is the peak initial response to 300 μM ACh \pm 10 μM azietomidate; I_f is the current after 1.95 sec. The observed recovery was fit to a single exponential: $I = I_{\text{rec}} - a_s \exp^{-bt}$, with I_{rec} , the current after full recovery; a_s , the amplitude of the observed, slow recovery on the time scale of seconds; and b , the rate constant. The amplitude of the rapid phase of recovery, a_r , is equal to $I_{\text{rec}} - (a_s + I_f)$. **Panels B and C**, experimental traces from two patches. The black traces are the ACh controls (1.95 sec exposure to 300 μM ACh, followed by recovery in buffer with test pulses of 300 μM ACh), and the gray traces are the

currents seen during exposure to ACh + 10 μ M azietomidate, followed by recovery in buffer alone (B) or in a stream containing 10 μ M azietomidate (C), with recovery tested by exposure to 300 μ M ACh and 10 μ M azietomidate. Traces shown in Panels B and C are the average of 4-6 sweeps each with 20-30 seconds between each sweep. The parameters characterizing the recovery kinetics are detailed in Table 1.

Figure 4. Comparison of nAChR inhibition by the open channel blocker QX-222 (100 μ M, A and B) and by azietomidate (10 μ M, C and D). *Torpedo* nAChRs were exposed simultaneously to 300 μ M ACh and inhibitor according to 4 different protocols that are numbered on the traces: (i) 800 ms of ACh, before return to buffer; (ii) 800 ms of ACh + inhibitor, before return to buffer; (iii) 30 msec of ACh + QX-222 (A) or 100 msec of ACh + azietomidate (C), before return to buffer; (iv) 30 msec of ACh + QX-222 (B) or ACh + azietomidate (D), before return to ACh alone for 170 msec. In each panel the bar above the current traces indicates the duration of exposure to ACh and QX-222 or azietomidate before switching the patch to a stream of buffer (A and C) or ACh (B and D). Panels A and B are all from a single patch, as are those from Panels C and D. Each trace is an average of 4 sweeps, with 20-120 seconds buffer wash between each trial.

Figure 5. Photolabeling in the nAChR α subunit transmembrane domain after 50 msec exposure to agonist and [3 H]azietomidate. nAChR-rich membranes (12 mg / condition) equilibrated without (Open, solid symbols) or with (Des, open symbols) 10 mM Carb were exposed to 10 μ M [3 H]azietomidate + 10 mM Carb for 50 ms prior to freezing and photolabeling. After photolabeling, V8 protease digests of the α subunits were fractionated by

SDS-PAGE and visualized by Coomassie blue stain, and material was eluted from the 10 kDa (α V8-10) and 20 kDa bands (α V8-20). The left hand panels are reversed-phase HPLC fractionations of (A) trypsin digests of α V8-10 samples (11,000 cpm injected each condition; recovery >90%) and (C) EndoLys-C digests of α V8-20 (●, 17,300 cpm injected, ○, 9,600 cpm injected, 70% recoveries). Also included are the absorbance at 215 nm (dotted line) and the HPLC gradient (% organic). ^3H (●, ○) and PTH-amino acids (◇, □) released during sequence analysis of nAChR subunit fragments beginning near the amino terminus of (B) α M4 (pools of HPLC fractions 26-31 from A), and (D) α M2 (pools of HPLC fractions 29-31 from C). The primary amino acid sequences are shown above each panel. (B) Each sample contained α subunit fragments beginning at α Tyr-401 (Des, □, $I_0 = 23$ pmol; Open, $I_0 = 16$ pmol, not shown) and at α Ser-388 (Des, ◇, $I_0 = 46$ pmol; Open, $I_0 = 28$ pmol, not shown;). The major peak of ^3H release in cycle 3 indicated labeling of α Glu-390, and the minor peaks of ^3H release in cycles 12 and 25 indicated labeling of α Cys-412 within the fragments beginning at α Tyr-401 and α Ser-388, respectively. D, Each sample contained as the primary sequence the fragment beginning at α Met-243 at the N-terminus of α M2 (Open & Des (□), $I_0 = 2.9$ pmol). The peak of ^3H release in cycle 20 indicated labeling of α Glu-262. The pool of HPLC fractions 32-35 from panel C contained fragments beginning at α Ser-173 (9 pmol each condition) and at α Met-243 (7 pmol each condition) and a single peak of ^3H release in cycle 20.

Figure 6. Photolabeling in the nAChR δ subunit transmembrane domain after 50 msec exposure to agonist and [^3H]azietomidate. nAChR δ subunits isolated from the labeling described in Figure 5 were digested with EndoLys-C and fractionated by Tricine SDS-PAGE.

(A) The distribution of ^3H eluted from 5 mm bands of the gel (**Open**, ●, 26,800 cpm loaded, 14,600 recovered; **Des**, ○, 17,400 cpm loaded, 10,200 cpm recovered). The mobilities of the molecular mass markers are indicated above the graph. **B**, Reversed-phase HPLC fractionation of material eluted from gel bands 7-9 (●, 6,350 cpm injected, 6,000 recovered; ○, 4,060 cpm injected, 3,330 cpm recovered). Also included are the absorbance at 215 nm for the **Des** sample (solid line) and the HPLC gradient in percent organic phase (dashed line). The right hand panels are the ^3H (●, ○) and PTH-amino acids (□) released during sequence analysis of nAChR subunit fragments beginning at the amino terminus of (C) δM2 (pools of HPLC fractions 26-29), and (D) M1 (pools of HPLC fractions 22-24). (C) The primary sequence began at $\delta\text{Met-257}$ at the N-terminus of δM2 (**Op**, $I_0 = 61$ pmol, not shown; **Des**, □, $I_0 = 60$ pmol) and secondary sequences began at $\delta\text{Asn-437}$ (**Open**, 21 pmol; **Des**, 20 pmol) and $\delta\text{Phe-206}$ (**Open**, 3.7 pmol; **Des**, 2.8 pmol). The peak of ^3H release in cycle 20 was consistent with labeling at $\delta\text{Gln-276}$ from the primary sequence detected. **D**, The primary sequence began at $\delta\text{Phe-206}$ before δM1 (**Open**, $I_0 = 30$ pmol, not shown; **Des**, □, $I_0 = 29$ pmol). The peak of ^3H release in cycle 31 indicated labeling of $\delta\text{Cys-236}$.

Figure 7. Photolabeling after rapid-freezing of nAChRs equilibrated with [^3H]azietomidate and agonist. ^3H (●, ○) and PTH-amino acids (■, □) released during sequence analysis of nAChR subunit fragments beginning at the amino terminus of αM2 (A), δM2 (B), and βM2 (C). The primary amino acid sequences are shown above each panel. nAChR-rich membranes (12 mg / condition), pre-equilibrated with 18 μM [^3H]azietomidate either without (solid symbols) or with (open symbols) 10 mM Carb, were exposed to 10 mM Carb for 50 ms and then rapidly frozen for photolabeling. As described in Experimental Procedures, the fragments containing

α M2 were isolated by reversed-phase HPLC from EndoLys-C digests of α V8-20; the fragments containing δ M2 or β M2 were isolated from an EndoLys-C digests (δ subunit) or trypsin digests (β subunit) by Tricine-gel SDS-PAGE followed by reversed-phase HPLC. **A**, The primary sequence began at α Met-243 (■, $I_0 = 2.7$ pmol; □, $I_0 = 1.2$ pmol), and the peak of ^3H release in cycle 20 indicated labeling of α Glu-262. **B**, The primary sequence began at δ Met-257 (□, $I_0 = 22$ pmol; not pre-equilibrated with Carb, $I_0 = 19$ pmol (not shown)). The ^3H release in cycle 20 indicated labeling at δ Gln-276. **C**, The primary sequence began at the N-terminus of β M2 (■, $I_0 = 9.2$ pmol) and a secondary sequence began at β Lys-216 at the N-terminus of β M1 ($I_0 = 5.1$ pmol, not shown). The ^3H release in cycle 20 indicated labeling at β Asp-268.

Figure 8. The binding sites for [^3H]azietomidate in the nAChR. Views of the *Torpedo* nAChR structure (Protein Data Bank Code 2BG9) (α , gold; β , blue; γ , green; δ , magenta) showing α -helical (cylinders) and β -sheet (ribbon) secondary structure. **A**, a perspective parallel to the membrane surface (with the γ subunit omitted); **B**, an expanded view of **A** focused on the top of the channel (γ and α_8 omitted); **C**, the transmembrane helices viewed looking down the ion channel; **D**, the δ subunit helix bundle looking down the M1 helix; **E**, the amino acid sequences of each of the M2 helices of the nAChR structure, with the amino acids highlighted in the structures indicated by the same colors. The residues labeled by [^3H]azietomidate are shown in stick format, color-coded for location: ion channel (position M2-20 (α Glu-262, β Asp-269; and δ -Gln-276; red); the δ subunit helix bundle (δ Cys-236, white); α M4 (α Cys-412; cyan); the cytoplasmic basket formed by the MA helices (α Glu-390, cyan). Also indicated in stick format in the M2 helices are unlabeled acidic side chains (β Glu-273 and δ Glu-280; green) that project

into the channel lumen and the prolines (*orange*) that precede those positions in each subunit. δ Phe-232 (*yellow*), the amino acid in δ M1 that is photolabeled by [125 I]TID (Arevalo *et al.*, 2005) and [3 H]benzophenone (Garcia *et al.*, 2007), is included, as are the amino acids in α MA/ α M4 (α Glu-398, α Asp-407, *purple*) photolabeled by [3 H]azicholesterol (Hamouda *et al.*, 2006). The volumes defined by the ensemble of the 10 lowest energy orientations of azietomidate docked at the extracellular end of the ion channel (grey, 680 Å³), in the δ subunit helix bundle (blue, 570 Å³), and in the cytoplasmic basket (yellow, 970 Å³) are shown in Connolly surface representations with a single azietomidate docked in its lowest energy orientation in each pocket (Experimental Procedures).

Figure 9. An azietomidate binding pocket in the nAChR cytoplasmic domain. (A) An alignment of the sequences of the *Torpedo* nAChR subunit and human 5-HT_{3A} receptor MA/M4 helices, with the positions in the nAChR α subunit photolabeled by [3 H]azietomidate, [3 H]azicholesterol (Hamouda *et al.*, 2006), and [3 H]azioctanol (Pratt *et al.*, 2000) colored *cyan*, *purple*, and *brown*, respectively. Other acidic and basic amino acids are colored *red* and *blue*, respectively. The positions in the 5-HT_{3A} receptor identified as conductance determinants are *green* (Hales *et al.*, 2006). (B) A Connolly surface representation of the basket formed by the MA helices, viewed from the side with the β and δ subunits removed to visualize the interior and with the amino acids color-coded as in (A). An azietomidate molecule in stick format is included docked in its lowest energy orientation (Experimental Procedures).

TABLE 1

Kinetics of recovery of ACh responses after inhibition by azietomidate. nAChRs in detached patches were exposed for 2 sec to 300 μ M ACh \pm 10 μ M azietomidate, and then returned to buffer, with ACh sensitivity monitored at intervals by moving the patch for 50 msec to a test solution of 300 μ M ACh + azietomidate (Figure 3). I_0 is the peak initial response to 300 μ M ACh \pm 10 μ M azietomidate; I_f is the current after 1.95 sec. The observed recovery was fit to a single exponential: $I = I_{rec} - a_s \exp^{-bt}$, with I_{rec} , the current after full recovery; a_s , the amplitude of the observed, slow recovery on the time scale of seconds; and b , the rate constant. The amplitude of the rapid phase of recovery, a_f , is equal to $I_{rec} - (a_s + I_f)$. See Figure 3A for a definition of the parameters.

	I_0 (pA)	I_f/I_0	I_{rec} (pA)	a_s (pA)	$\tau_s = b^{-1}$ (msec)	a_f (pA)
Figure 3B						
ACh	220	0.31	206 \pm 1	115 \pm 1	770 \pm 20	21.4
ACh + azi	241	0.02	228 \pm 2	161 \pm 4	470 \pm 30	61.6
Figure 3C						
ACh	226	0.27	204 \pm 1	116 \pm 1	880 \pm 40	27.9
ACh + azi	239	0.002	220 \pm 10	129 \pm 15	570 \pm 190	90.5

TABLE 2

State dependence of [³H]azietomidate photoincorporation into residues in the nAChR transmembrane domain (cpm/pmol of PTH-derivative)^a.

	50 msec [³ H]azietomidate (Figs 5 and 6)		Equilibrium [³ H]azietomidate (Figure 7)	
	Carb 50 msec	Carb Equilibrium	Carb 50 msec	Carb Equilibrium
Ion channel				
αM2-20 (αGlu-262)	25	13	67	42
δM2-20 (δGln-276)	1.0	0.5	1.7	1.0
δM2-24 (δGlu-280)	<.04	<.03	<0.1	<0.1
βM2-20 (βAsp-268)	ND	ND	4	ND
βM2-24 (βGlu-272)	ND	ND	<0.2	ND
δM1				
δCys236	0.7	0.2	2	2
αMA/αM4				
αGlu-390	1.2	0.6	ND	ND
αHis-408	0.2	0.2		
αCys412	0.8	0.4		

^aThe level of ³H incorporation in each residue was calculated from the observed ³H release as described in Experimental Procedures, and the mass was calculated from the initial and repetitive yield. ND, not determined

Figure 1

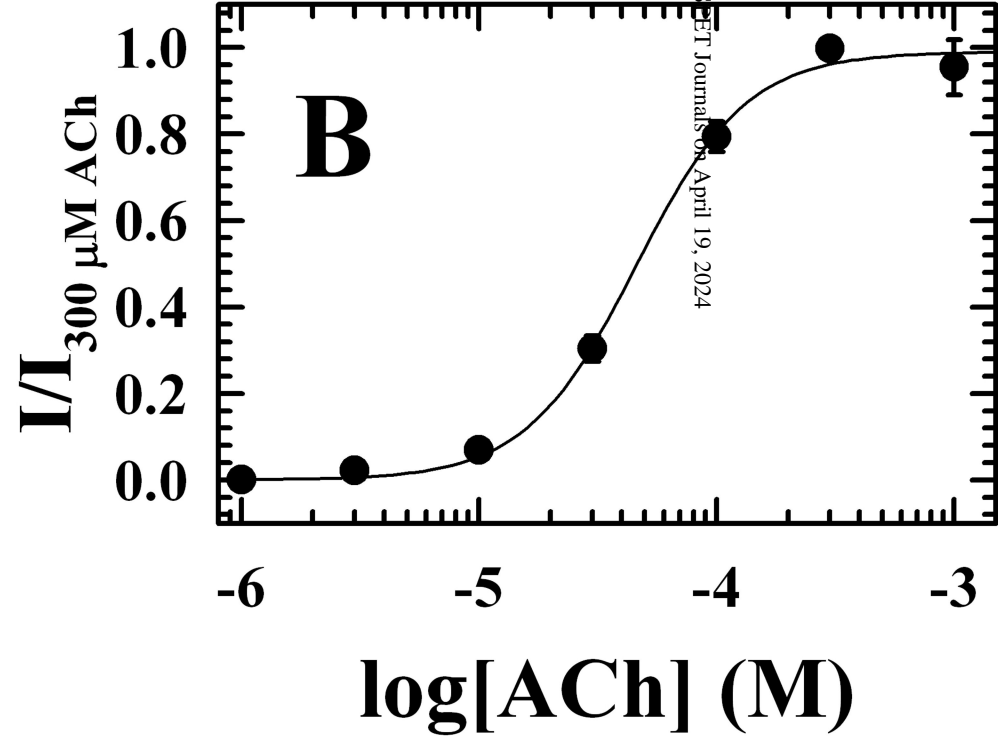
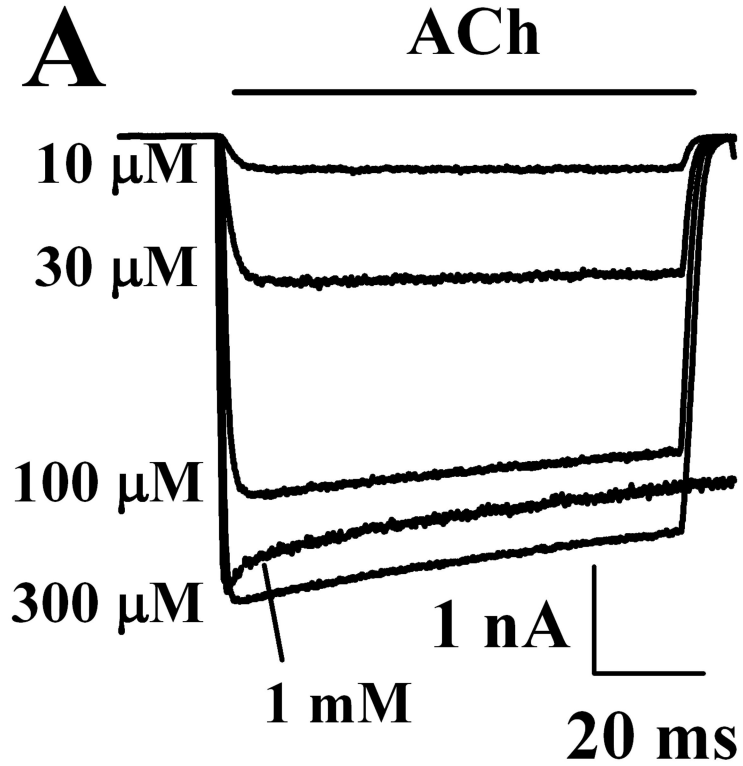


Figure 2

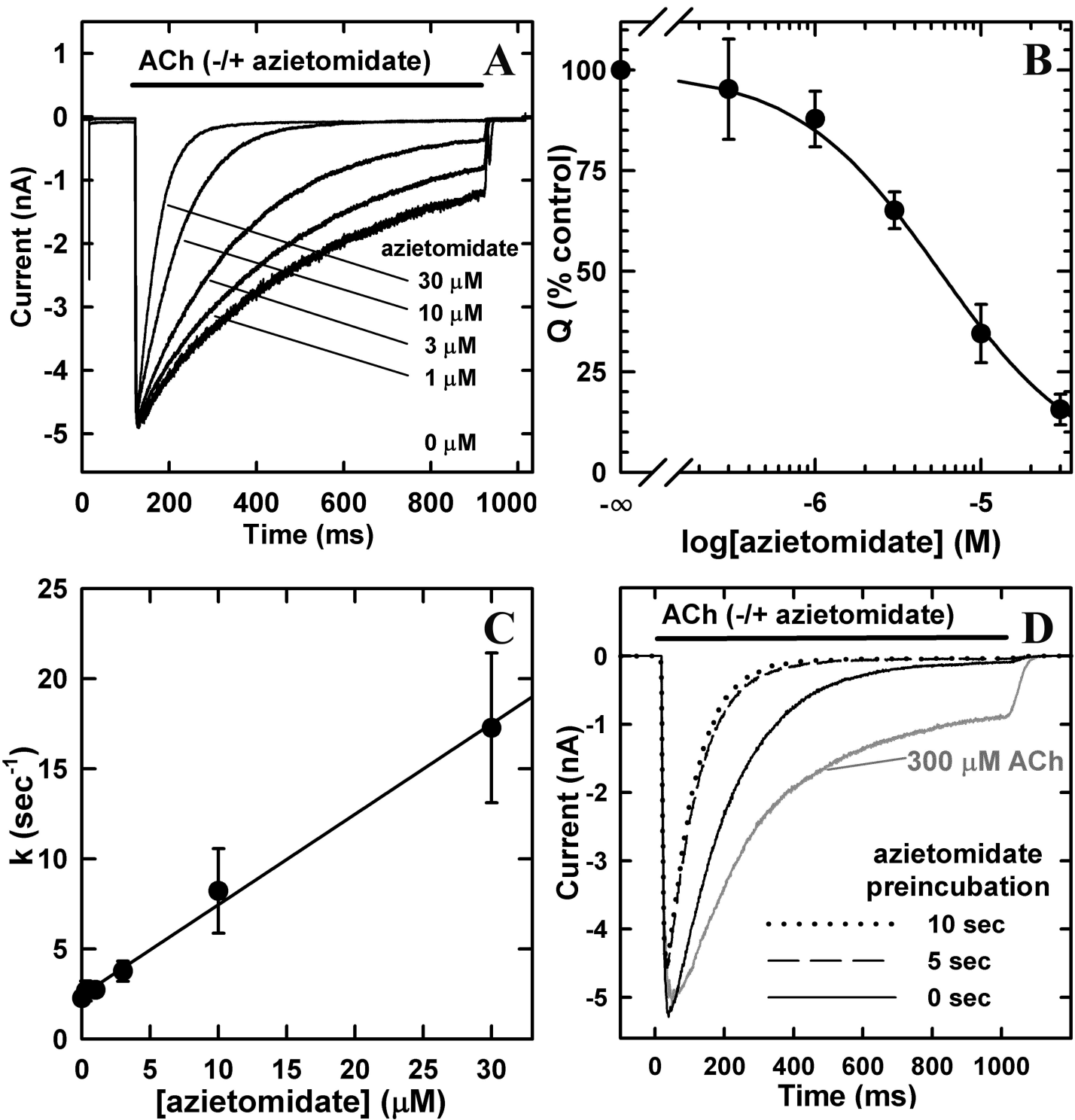


Figure 3

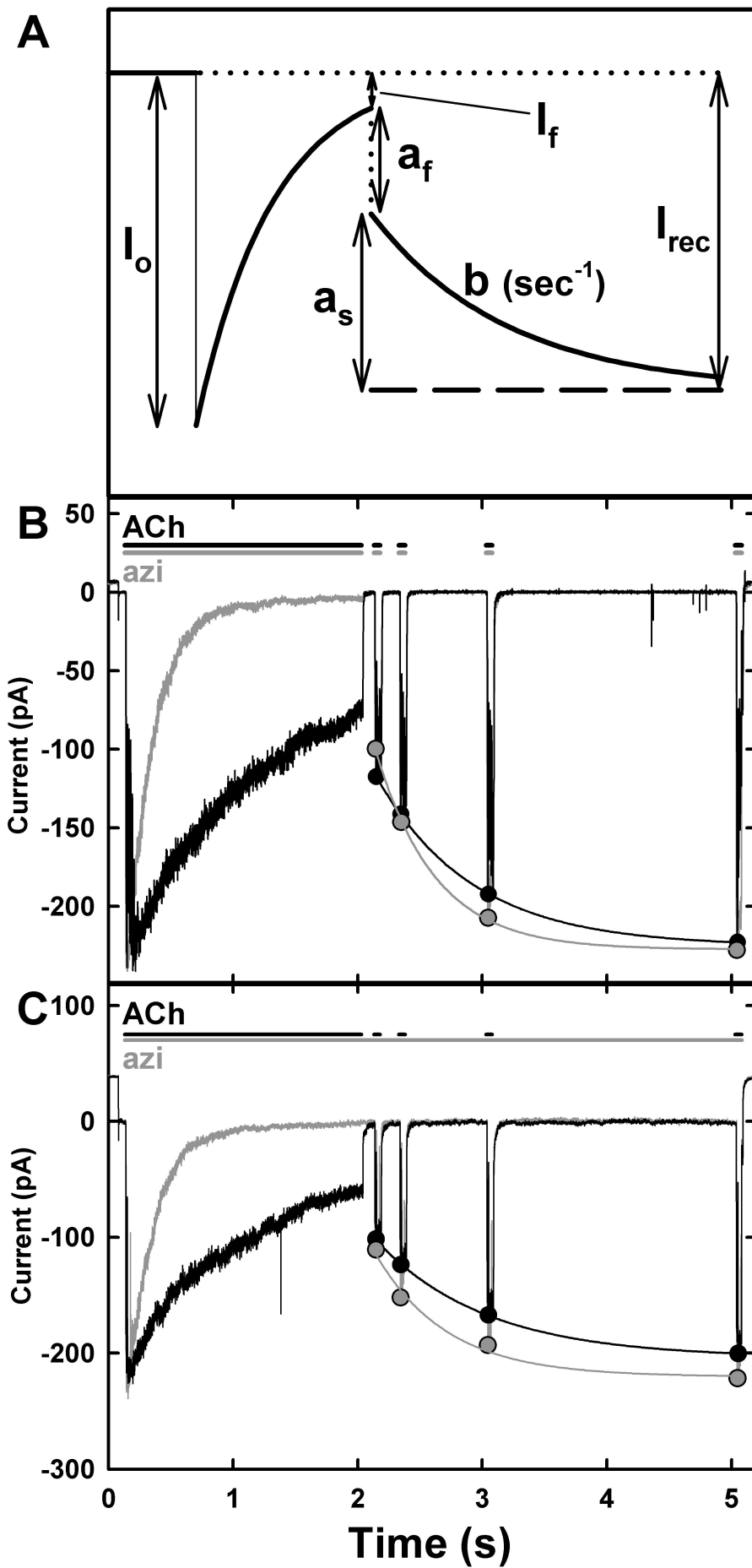


Figure 4

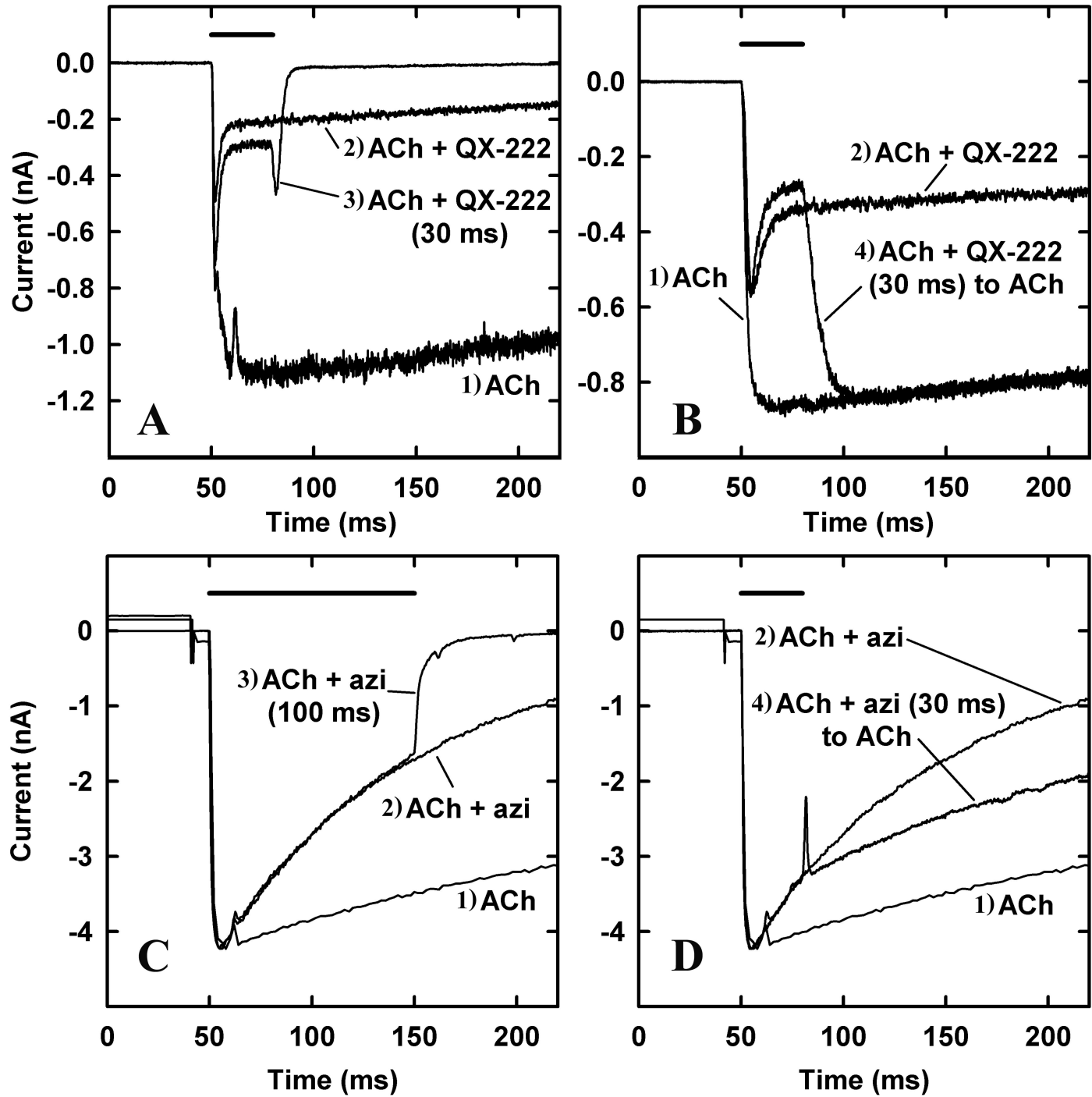
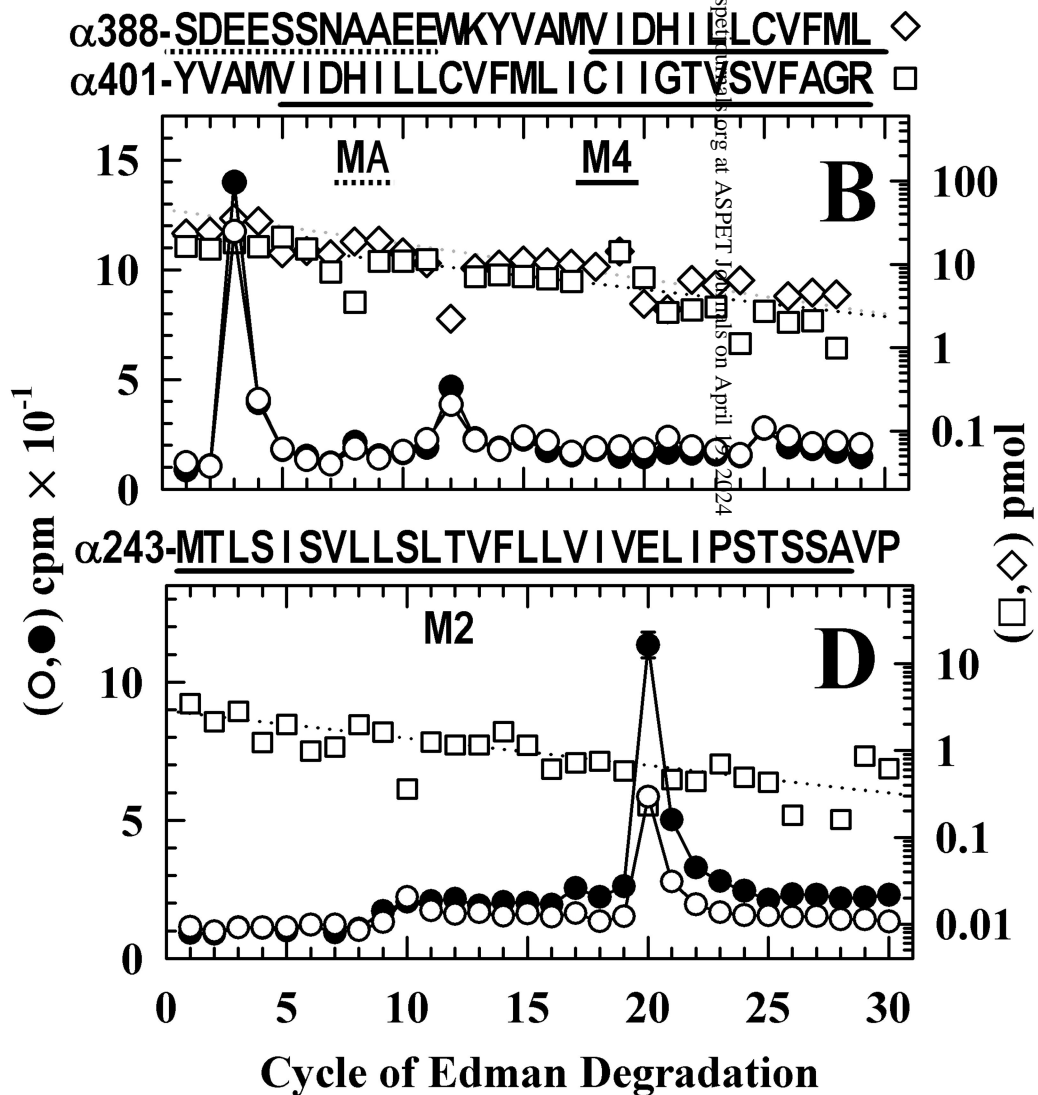
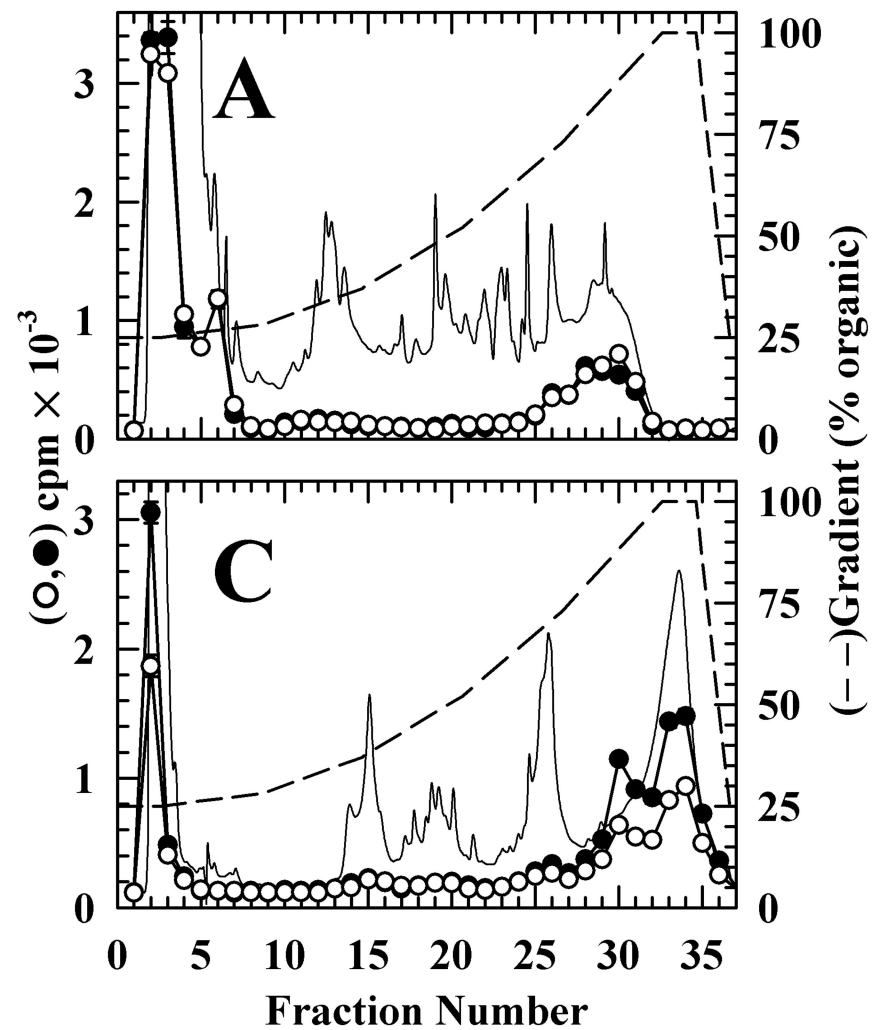
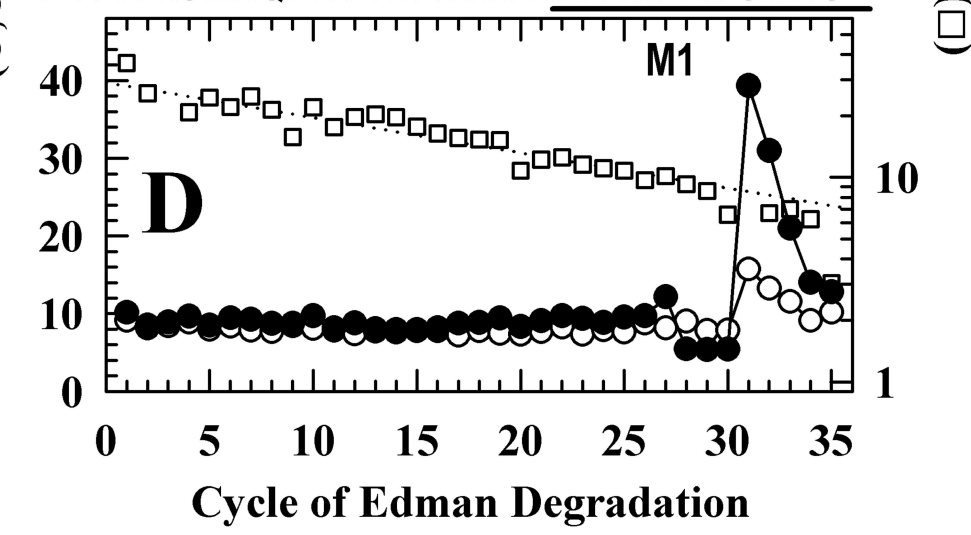
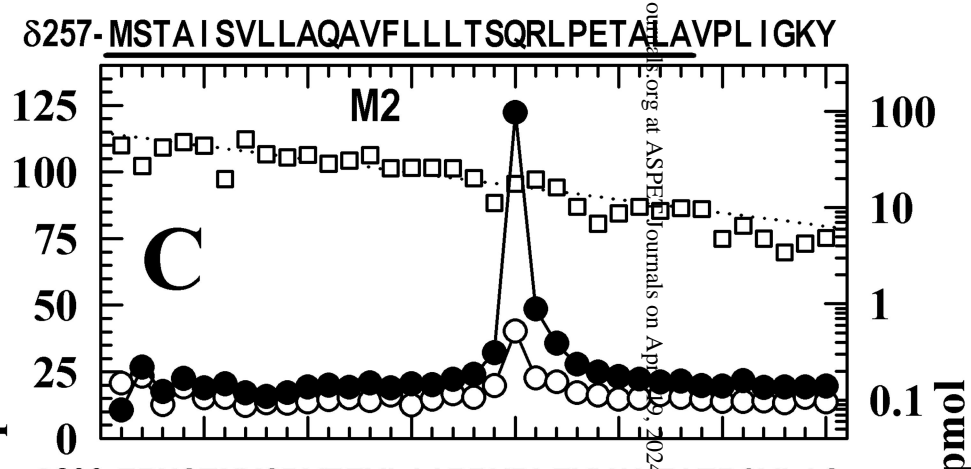
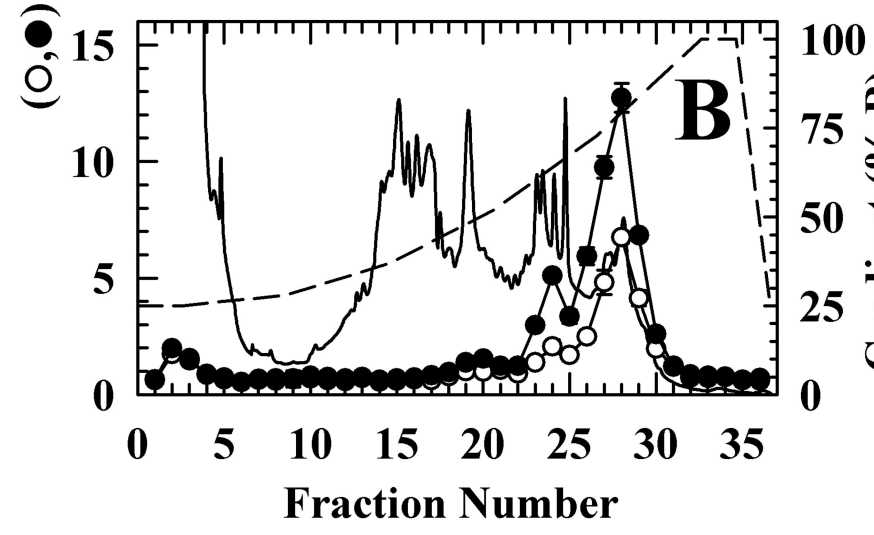
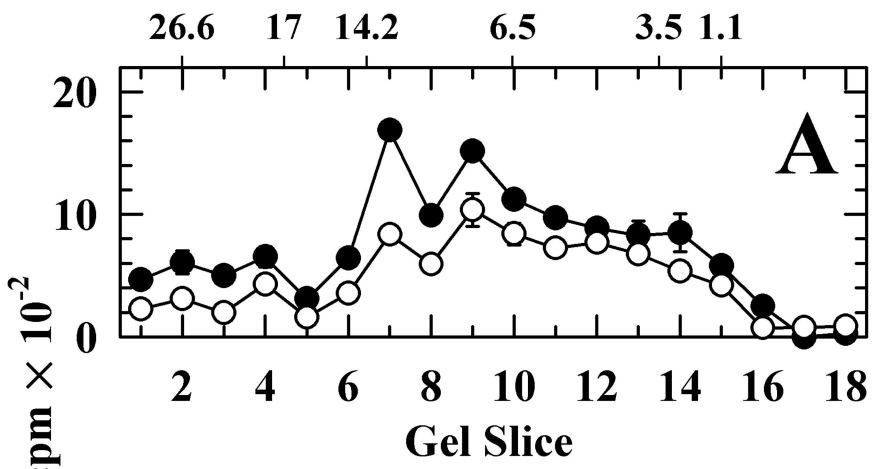


Figure 5



Downloaded from molpharm.aspet.org at ASPET Journals on April 19, 2024

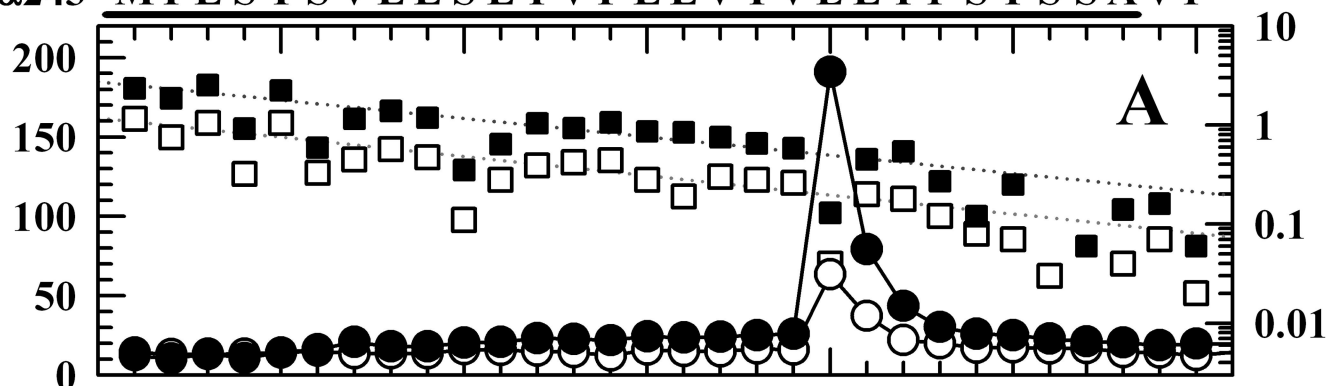
Figure 6



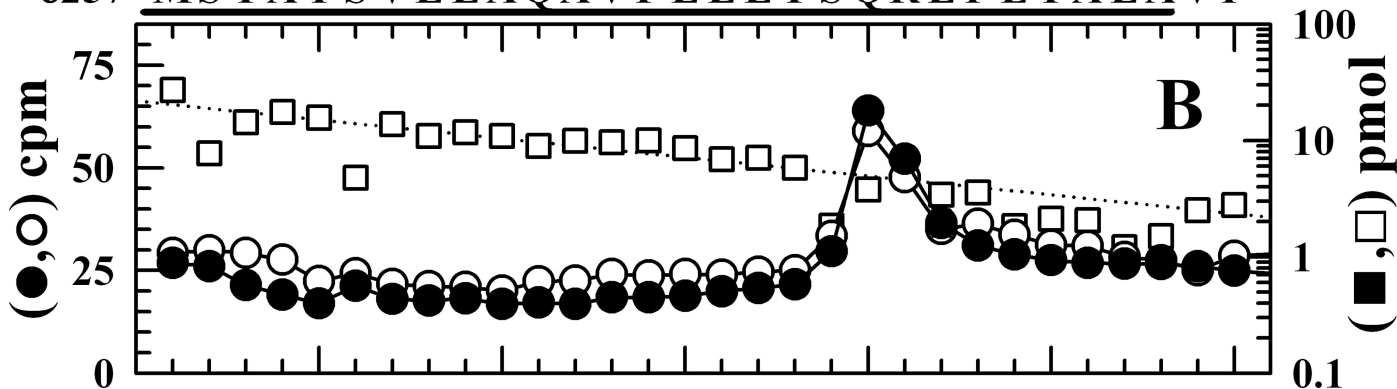
Downloaded from molpharm.aspetjournals.org at ASPET Journals on April 29, 2012

Figure 7

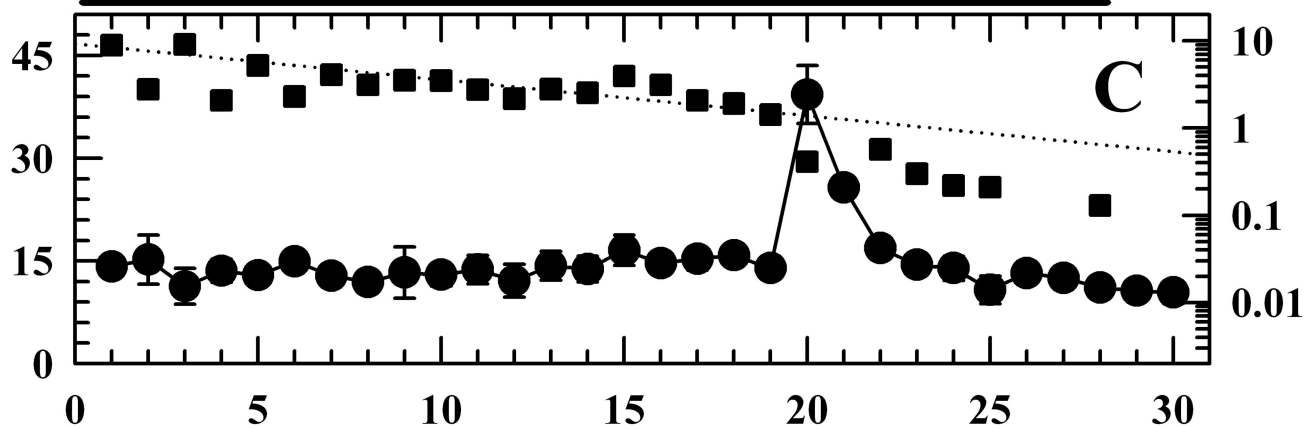
α 243- MTLSISVLLSLTVFLLVIVELIPSTSSAVP



8257- MSTAISVLLAQAVFLLLSQRLPETALAVP



β 249- MSLSISALLAVTVFLLLLADKVPETSLSVP



Cycle of Edman Degradation

Figure 8

